ACS OMEGA

http://pubs.acs.org/journal/acsodf

Article

Flexible Nano-TiO_2 Sheets Exhibiting Excellent Photocatalytic and Photovoltaic Properties by Controlled Silane Functionalization—Exploring the New Prospects of Wastewater Treatment and Flexible DSSCs

Soorya Sasi, Akash Chandran, Sunish K. Sugunan, Ardra C Krishna, Pankajakshan Radhakrishnan Nair, Aneena Peter, Arsha N. Shaji, Kavasseri. R. V. Subramanian, Narendra Pai, and Suresh Mathew*

Cite This: *ACS Omega* 2022, 7, 25094−25109

Read Online

ACCESS | Metrics & More | Article Recommendations | Supporting Information

ABSTRACT: TiO_2 nanoparticles surface-modified with silane moieties, which can be directly coated on a flexible substrate without the requirement of any binder materials and postsintering processes, are synthesized and characterized using X-ray diffraction, Fourier transform infrared spectroscopy, scanning electron microscopy, Brunauer−Emmett−Teller, X-ray photoelectron spectroscopy, Raman spectroscopy, photoluminescence spectroscopy, time-correlated single-photon counting, and transmission electron microscopy. The viability of the prepared surface-modified TiO_2 (M-TiO_2) sheets as a catalyst for the photo-induced degradation of a model dye, methylene blue, was checked using UV−visible absorption spectroscopy. The data suggest that, compared to unmodified TiO_2, M-TiO_2 sheets facilitate better dye-degradation, which leads to a remarkable photocatalytic activity that results in more than 95% degradation of the dye in the first 10 min and more than 99% of the degradation in the first 50 min of the photocatalytic experiments. We also demonstrate that M-TiO_2 can be recycled with negligible reduction in photocatalytic activity. Further, the photovoltaic properties of the developed M-TiO_2 sheets were assessed using UV−visible absorption spectroscopy, electrochemical impedance spectroscopy (EIS), and photochronoamperometry. Dye-sensitized solar cells (DSSC) fabricated using M-TiO_2 as the photoanode exhibited a photoconversion efficiency of 4.1% under direct sunlight. These experiments suggested that M-TiO_2 sheets show enhanced photovoltaic properties compared to unmodified TiO_2 sheets, and that, when N-719 dye is incorporated, the dye−TiO_2 interaction is more favorable for M-TiO_2 than bare TiO_2. The simple solution processing method demonstrated in this paper rendered a highly flexible photoanode made of M-TiO_2 with superior charge-separation efficiency to an electrode made of bare TiO_2. We propose that our findings on the photovoltaic properties of M-TiO_2 open up arenas of further improvement and a wide scope for the large-scale production of flexible DSSCs on plastic substrates at room temperature in a cost-effective way.

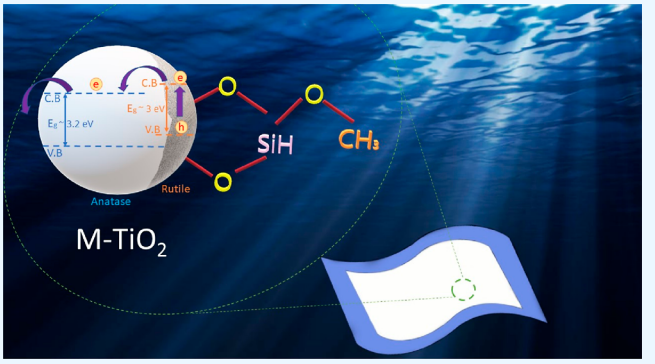

INTRODUCTION

The holy grail of research in the fields of photocatalytic and photovoltaic conversion is a means for effective utilization of photo-generated excitons, including their quantitative separation into charge carriers, which has been a key factor in deciding the efficiencies of these processes. Efforts to develop suitable candidates that can act as potential light sensitizers and/or an intermediate system that facilitates charge separation culminated in the development of multitudes of organic dye molecules and nanostructures. Of them, TiO_2 nanoparticles, which could serve both the abovementioned roles, have already revolutionized the fields of photocatalysis[1] and photovoltaics;[2] as evidenced by large numbers of research articles published each year on the use of TiO_2 nanoparticles in both areas. In particular, the optoelectronic properties of both anatase and rutile polymorphs of TiO_2 have been intensely investigated for the prospects of using it in light-energy conversion applications.[3−5] TiO_2 is widely accepted as an n-type semiconductor with a wide indirect band gap.[6] Photoexcitation of anatase TiO_2 has been reported to generate a large number of strongly bound excitons that display an intermediate character between the Wannier−Mott and Frenkel excitons, that hold a two-dimensional wave-like

Received: March 9, 2022
Accepted: June 28, 2022
Published: July 13, 2022

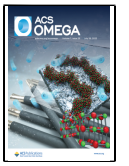

nature,[7] and are confined in the 001 planes in the 3-dimensional lattice.[8] In addition, the critical carrier density, which governs the dissociation of strongly bound excitons into uncorrelated electron−hole pairs, for exciton Mott transition in photodoped anatase TiO_2 is found to have a remarkably high magnitude. In rutile TiO_2, on the other hand, photoexcitation results in weekly bound excitons that are of the Wannier−Mott character.[9] These excitonic properties, which largely govern events that lead to the formation of charge carriers, along with the excellent electron-transport[10] and electrical properties,[11] make nano-TiO_2 an appealing candidate for both photocatalytic and photovoltaic applications.

If devices employed for these applications are flexible, instead of being rigid, it will be more advantageous from an operational point of view. Recently, in the optoelectronic field, flexible devices[12] surged as fascinating new candidates that offer the unique advantage of malleability which makes carriage and installation of the devices on surfaces of any morphology easy where conventional solid-state devices fail because of their rigid and brittle nature.[13] On one hand, if TiO_2 nanoparticles are to be used in wastewater purification, from a practical point of view, it is desirable to make the TiO_2-based photocatalytic sheet as flexible as possible, so that the water purifier can be operated under any mechanical conditions. On the other hand, to make mechanically flexible dye-sensitized solar cells (DSSCs), it is imperative to have its components, if not all, including the photoanode, in a flexible morphology.[14]

In DSSC applications, in general, TiO_2 is coated onto a rigid/flexible substrate which improves the morphology, design, and hence, the performance of the device.[15] For making a TiO_2-based photoanode in DSSCs,[16] the procedure of coating requires that the TiO_2 be made into a paste by adding suitable organic species, such as polymer binders, which are typically required to make the photoanode films crack-free. The TiO_2 film thus made is required to be calcinated at high temperatures to make the TiO_2 well-adherent onto the substrate and to remove the residual polymer from the film. In addition, the calcination process eliminates the charge transfer inhibition caused by the nonconducting polymer additive and improves the optoelectrical properties of the photoanode film.[17] However, when flexible plastic sheets are to be used as substrates of the photoanode material in a DSSC scheme, calcination poses a problem as it could degrade the plastic substrates at high temperatures, which could affect the morphology, and hence, the efficiency of the device. Though annealing of the system at a lower temperature can afford the retention of the substrate, it does also retain some fraction of the binder polymer as well, which could pose a barrier to the charge transfer process. Therefore, it is highly desirable to develop a flexible TiO_2-based photoanode material that can be coated directly onto flexible plastic sheets without the requirement of a binder polymer, so that a crack-free coating that adheres well to the substrate can be obtained without a calcination process. A lot of research is being carried out worldwide to develop low-temperature fabrication methods of TiO_2 photoanodes for flexible DSSCs. Lin *et al.*[18] developed a binder-free TiO_2 photoanode coated on Ti sheets at a low annealing temperature of 120 °C and achieved a photoconversion efficiency of 3.4%. In another article, Zeng *et al.*[19] made a TiO_2 photoanode with hydroxypropyl methylcellulose as a binder material. The binder material was made to degrade by 10 h of UV light treatment followed by annealing at 150 °C to obtain entirely flexible TiO_2 sheets. They achieved a photocurrent conversion efficiency of 3.25%. Holliman *et al.*[20] synthesized a TiO_2 photoanode material with hexafluorotitanic acid as a binder and fabricated a TiO_2 photoanode by sintering these materials at 119 °C followed by treating the anode with $TiCl_4$, and by carrying out a re-sintering at 119 °C. DSSC fabricated using this photoanode showed a photoconversion efficiency of 4.2%. Lee *et al.*[21] fabricated a DSSC with a hierarchically structured TiO_2 (HS-TiO_2) on a flexible indium tin oxide (ITO)-polyethylene naphthalate substrate *via* an electrospray deposition method and achieved a photoconversion efficiency of 5.57%.

Most of the articles, where fabrication of TiO_2-based flexible DSSC has been discussed, show efficiencies between 0.1 and 8%, where the highest efficiency reported fabrication requires many pre/post-treatments such as ball-milling process and mechanical pressing. Toward the objective of developing flexible TiO_2 sheets, some articles reported the preparation of secondary mesoporous TiO_2 nanoparticle aggregates with primary anatase nanocrystallites as photoelectrode through the electrophoretic deposition method.[22] However, this method was proven to be impractical for large-scale productions. Another report introduced a lift-off technique, in which a layer of presintered porous TiO_2 on a glass substrate was transferred to an arbitrary second, flexible substrate at high pressure.[23] All of the methods described above are cumbersome, require sophisticated production machinery, and are not suitable for production on large scales. These difficulties demand the need for a simple and convenient solution-processable method that is manageable for large-scale production requirements. Nonvolatile functional molecular gels/liquids prepared *via* surface modification with long aliphatic chains or bulky aromatic functional moieties[24] and that exhibit less viscosity at room temperature were proposed as potential candidates for optoelectronic and electrochemical device preparation and applications in the energy harvesting/storage and water purification fields.[25] These materials, when being used in synthesizing a solvent-free slurry, offer the unique advantage that no solvent is required for making the active material so that solvent evaporation problems that may arise from using a solvent in a device can be eliminated. This new approach for preparing functionalized organic and inorganic nanostructures with liquid-like behavior is reported in several recent articles.[26] Bourlinos *et al.* synthesized a solvent-free viscous nanofluid of anatase TiO_2,[27] where poly(ethylene)glycol (PEG)-functionalized sulfonate anion $C_9H_{19}-C_6H_4-O(CH_2CH_2O)_{20}SO_3^-$ was used as a canopy. In another article, Yu *et al.* discuss the synthesis of a solvent-free nanofluid of TiO_2 nanoparticles by surface modification using trimethoxysilane.[28] TiO_2 nanoparticles coated with the organic canopy showed better dispersion after modification. The same team also studied the properties of nanofluid in another article and they found that as the temperature decreases below 10 °C, the nanofluid turned into a waxy-solid form. Zheng *et al.* synthesized solvent-free gold nanofluids by grafting thiol 11-mercaptoundecanoic acid onto a gold-nanoparticle surface, followed by self-assembly with a PEG-substituted tertiary amine.[29] Other well-known photocatalysts like ZnO/ZrO_2 nanofluids[30] were also prepared using similar surface modification strategies. A multitude of articles[31−34] report the synthesis of silane-modified TiO_2 through various routes, its rheological properties, its adhesive nature on various substrates, and so forth. However, of these articles, only a handful discuss the possibility of using silane-modified TiO_2 in photocatalysis.

https://doi.org/10.1021/acsomega.2c01425
ACS Omega 2022, 7, 25094−25109

Table 1. Summary of Silane-Modified TiO_2 in Photocatalytic Wastewater Treatment and Environmental Applications

coupling agent used	model pollutant	remarks	refs. no
APTES	Cr(VI)	pH plays a crucial role in the absorption of chromium. Optimization of pH, contact time, and concentration leads to maximum absorption	51
APTES	MB	calcination plays a key role in tuning the photocatalytic ability of the silane-coupled TiO_2 photocatalyst. The calcination changed the zeta potential of the modified TiO_2 photocatalyst. Calcination above 300 °C increased the photocatalytic ability and stability of the material	35
APTES	MB, orange II	the adsorption has a significant impact on the photooxidation of dyes. The APTES/TiO_2 photocatalysts calcined at 900 °C showed high degradation rates. Functionalization *via* APTES suppressed the anatase-to-rutile phase transition, as well as the growth of the crystallite size	36
APTES	MB	the presence of Si and C in the APTES-modified TiO_2 contributed to effective inhibition of the anatase-to-rutile phase transformation and the growth of the crystallite size of both polymorphous forms of TiO_2 during calcination at high temperature	39
vinyltriacetoxysilane	rhodamine B	a large amount of modifier in the silane-modified TiO_2 reduced the photocatalytic ability of the TiO_2	40
octadecyl trichlorosilane	rhodamine B	in the case of modified TiO_2, a direct electron transfer to the conduction band of TiO2 upon absorption of UV light was facilitated by the organic chain with an optimum length	41
APTES, 3-isocyanato propyl trimethoxy silane (IPTMS)	malachite green	a high silane modifier concentration negatively affected the photocatalytic ability	42
propyltrimethoxysilane, triethoxy(octadecyl)silane, trimethylchloro-silane	nitric oxide	silane-modified TiO_2 paint showed significant improvement in NO reduction than that of the unmodified sample and showed good self-cleaning properties	31
γ-aminopropyltriethoxy silane (APTES), γ-amino propyltrimethoxy silane (APTMS), *N*-(2-aminoethyl)-3-amino propyltriethoxysilane (AEAPTES)	brilliant red X-3B	the degradation of the dye was 96.4% after 180 min of light irradiation. Doping of Si into the TiO_2 effectively delayed the anatase-to-rutile phase transition, prevented the growth of titania grains, and increased surface area and UV light-induced photocatalytic activity	43
3−9(trimethoxysilyl)propylmethacrylate (KH570)	heavy metals, phenol, poly-brominated diphenyl ethers (PBDEs)	Degradation of the dye was observed at 93% after 4 h of irradiation. Due to the self-condensation effect of the silane modifier, a considerable amount of silicon hydroxyl was provided as the hole trapping agent, thus improving the ability of the catalyst	44
APTES	heavy metals like Cu^{2+}, Cd^{2+}, and Pb^{2+}	Adsorption capacities of APTES-modified hollow TiO_2 nanospheres for Cu^{2+}, Cd^{2+}, and Pb^{2+} ions were found to be 12.7, 17.5, and 1.8 times more than those of unmodified samples respectively	45

https://doi.org/10.1021/acsomega.2c01425
ACS Omega 2022, 7, 25094−25109

One of those research articles reports[51] the photocatalytic activity of TiO_2 surface modified with 3-aminopropyltriethoxysilane (APTES) in degrading the methylene blue (MB) dye to an extent of 88% after 240 min of light irradiation. In another report, the role of adsorption and calcination in the photocatalytic degradation of the MB dye in the presence of APTES modified TiO_2 was investigated, in which a maximum of 96% degradation percentage after 240 min of irradiation was reported.[35,36] Takeshita[37] has carried out computational studies at the density functional theory (DFT) and time-dependent-DFT levels on an azobenzene-based dye covalently attached to silane coupling agents (SCAs). The SCAs were coupled to a terminal oxirane group of the photosensitizing dye containing a 1-naphthylamine moiety, and it was found that the CH−O interactions can be utilized to regulate the geometry of the dye to achieve characteristics favorable for electron injection into the conduction band of TiO_2. Ukaji *et al.*[38] investigated the effect of surface modification with APTES and *n*-propyltriethoxysilane on the photocatalytic activity and UV-shielding ability of fine TiO_2 particles. They found that the number of surface functional groups (NR) and the density of SCAs modified on TiO_2 surface affected the photocatalytic ability and UV-shielding ability of modified TiO_2. An NR of 6.2 suppressed the photocatalytic activity by up to a factor of 25%. This indicates that optimizing the amount of the surface modifier positively affects the photocatalytic ability. Efforts were made to use silane-modified TiO_2 in photocatalytic dye degradation,[39] and attempts are being made to improve their photocatalytic efficiency. The details of the state of the art of research on silane-modified TiO_2 in photocatalytic dye degradation are summarized in Table 1.

In this article, we investigate the optical and electrochemical characteristics of nano-TiO_2 flexible sheets prepared by the surface functionalization of TiO_2 nanoparticles with trimethyloxysilane followed by a double sintering process and its application in wastewater treatment and photovoltaics. To the best of our knowledge, our work reports the best performing silane-modified TiO_2 flexible photocatalyst sheet that decomposes the MB dye to more than 95% extent within the first 10 min of irradiation, and to more than 99% within less than an hour of irradiation, which is a significantly greater improvement over bare TiO_2, which is capable of decomposing the dye to a maximum of 68% (*vide infra*). In a nutshell, we demonstrate that the prepared nano-TiO_2 sheets (M-TiO_2), compared to bare TiO_2, showcase superior photocatalytic activity and reasonably high photovoltaic properties at room temperature and show far better efficiency than that of other similar reported synthesis routes.[31]

EXPERIMENTAL SECTION

A detailed experimental section is provided in Supporting Information.[46−48]

Preparation of TiO_2 Nanoparticles. 7 mL of titanium(IV) butoxide was added dropwise into 15 mL of ethanol under continuous stirring. Following this, a mixture of 2 mL of HCl and 1 mL of deionized water in 15 mL ethanol was added to the titanium(IV) butoxide solution under continuous stirring for 6 h at room temperature. The as-obtained precipitate was washed with water and sintered at 450 °C for 5 h in the oven.

Preparation of Surface-Modified TiO_2 Nanoparticles (M-TiO_2). 0.25 g of the prepared TiO_2 nanopowder, 0.5 g of *n*-methyl glycine (sarcosine), and 0.5 g of trimethoxy silane were added to 100 mL of toluene and stirred for 24 h at 70 °C. The obtained material was washed with water and sintered at 450 °C for 5 h. The resultant powder was mixed with toluene, stirred for 5 h, and sintered at 450 °C to get the final product. The intermediate product without the final sintering process was selected as a control to find out the effect of stirring with toluene and double sintering. The intermediate product obtained was labeled as I-TiO_2 and its photocatalytic activity was compared with those of TiO_2 and M-TiO_2. When the sintering process was repeated more than 2 times, delamination of TiO_2 from the substrate occurred. M-TiO_2 samples with different trimethoxy silane contents were prepared. Trimethoxy silane weight percentages varying from 0, 0.25, 0.5, 1, and 5 g were taken and the M-TiO_2 preparation procedure was followed to get 5 samples with different silane contents and were labeled as 0, 1:1, 1:2, 1:4, and 1:20, respectively.

Photocatalysis. The photocatalytic efficiency of the catalysts, M-TiO_2, I-TiO_2, and TiO_2, were compared using a standard MB dye solution. A 20 ppm stock solution of MB solution was taken in three 100 mL labeled beakers and 80 milligrams of the catalysts were, respectively, added to each beaker. The MB solution without any catalyst was labeled as blank. After the addition of the catalysts, the samples were sonicated (230 V AC 50 Hz) for 5 min in dark to ensure uniform interaction of the dye and the catalysts. After sonication, each suspension of the solution was allowed to be exposed to intense sunlight (with a power of 970 W/m^2, a latitude of 9.669090, a longitude of 76.539070, and an elevation of 21 m). A 5 mL solution was collected from each sample solution at a 10 min interval until the solution turned colorless. The absorbance of the collected solution was analyzed using a UV−visible spectrometer at each time interval. The absorbance was measured at an observational wavelength of λ = 668 nm against a reference sample of deionized water using a Shimadzu UV-2450 spectrophotometer. The relative concentration of the dye before and during the catalysis process, C/C_0, was plotted against the time of irradiation for calculating the percentage of degradation. A free-radical scavenger study was also performed to identify the active species responsible for photocatalytic activity. For that purpose, three different scavengers such as $AgNO_3$ (electron scavenger), ethylene diamine tetra-acetic acid (EDTA) (hole scavenger), and isopropyl alcohol (IPA) (hydroxyl radical scavenger) were used. For evaluating the applicability of flexible M-TiO_2 sheets in photocatalysis, thin films of M-TiO_2 were prepared by grinding the as-synthesized M-TiO_2 nanopowder and ethanol with a mortar and pestle to make a fine paste, and the subsequent coating of the paste onto a polyethylene terephthalate (PET) sheet was done by using a doctor blading technique. Photocatalytic activity of the thin film of TiO_2 was also checked under identical conditions for comparison purposes (Videos S1 and S2 in Supporting Information). The photographs of the M-TiO_2 thin film before and after the dye degradation process are shown in Figure 1.

Photoanode Fabrication. M-TiO_2 was made into a paste by adding ethanol, ground with a mortar and pestle, and coated onto a flexible sheet of ITO-coated PET by a simple doctor blade technique. It should be noted that no polymer binder materials were employed during the coating process and no postsintering processes were conducted afterward. The thickness of the coating was measured using a MAHR precision

https://doi.org/10.1021/acsomega.2c01425
ACS Omega 2022, 7, 25094−25109

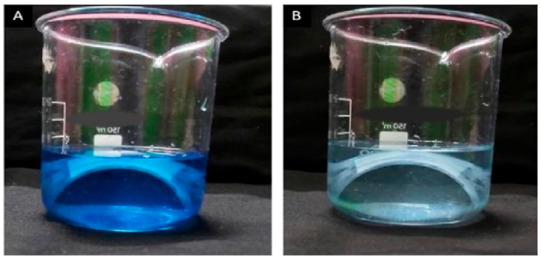

Figure 1. (A) M-TiO_2 coated PET sheet bent and immersed in dye solution before and (B) after the dye degradation.

outside micrometer 40A with a 0.01 mm least count and a range of 0−25 mm, and the thickness of the coating was found as 33 μm.

Cross-Cut Adhesion Test. A right-angle grid was cut into the coatings penetrating through to the substrate. The cuts were made at 45° with respect to the direction of the grain. A transparent pressure-sensitive tape was then placed over the lattice and rubbed with a fingertip to ensure good contact. The tape was removed by pulling it off steadily at an angle as close as possible to 60°. The cut area of the test coating was examined and is classified from 0 (good adhesion) to 5 (bad adhesion) by visual comparison with the illustrations in the standard, depending on the amount of flaked coating.

Preparation of Electrolytes. The (I_3^-/I^-) redox electrolyte was prepared by mixing 0.1 M potassium iodide, 0.5 M *tert*-butyl pyridine, 0.05 M iodine, and 0.4 M lithium perchlorate in acetonitrile. Cobalt electrolyte was prepared by adding 0.22 M tris(2-(1*H*-pyrazol-1-yl) pyridine) cobalt(II) tri[hexafluorophosphate] 0.05 M tris(2-(1*H*-pyrazol-1-yl)-pyridine) cobalt(III) di[hexafluorophosphate], 0.1 M $LiClO_4$, and 0.2 M 4-*tert*-butylpyridine in acetonitrile. Cobalt complexes were added into acetonitrile followed by TBP and $LiClO_4$ and stirred well under 50 °C for 30 min in a closed vial.

DSSC Assembly. Dye anchored M-TiO_2 photoanodes were cut into a 1 cm^2 square and a parafilm spacer was used as an insulator to cover the parts other than the exposed active area, and the electrolyte was filled inside the cell. Then a platinum counter electrode was sandwiched against the photoanode. The cells were sealed and connected to the electrochemical workstation for *IV* measurement by using crocodile clips.[49] Figure 2 shows the images of M-TiO_2-coated

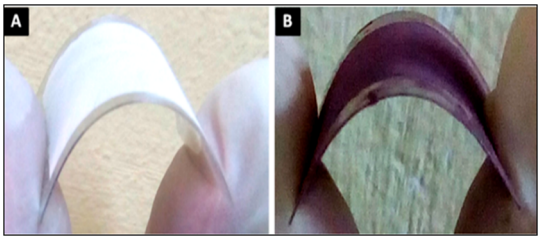

Figure 2. (A) As prepared M-TiO_2 coated ITO sheets and (B) after N-719 dye adsorption.

ITO flexible sheets without the dye (A) and with (B) dye adsorption. The M-TiO_2 nanoparticles when coated on ITO-PET sheets demonstrated excellent adhesion properties; which was evident from the observation that the coated film stuck on the substrate without any delamination even after repeated mechanical bending and twisting and extensive soaking in alcohol during the N-719 dye loading process.

RESULTS AND DISCUSSIONS

Morphology and Structural Analysis. *X-ray Diffraction.* X-ray diffraction (XRD) patterns of unmodified TiO_2[50] and M-TiO_2 are shown in Figure 3, where both the samples show the

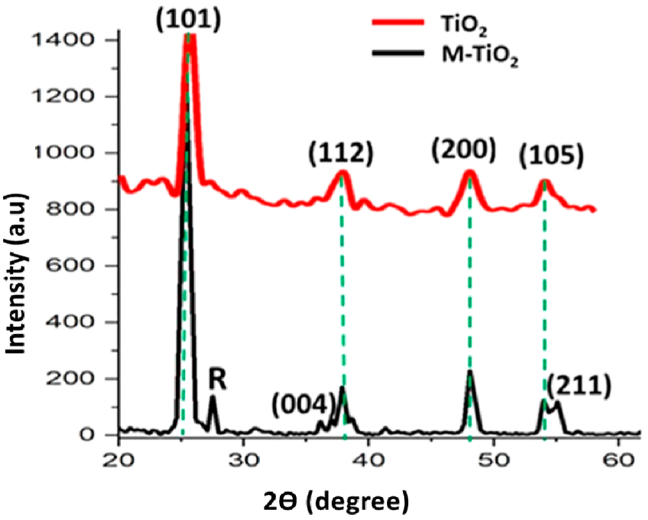

Figure 3. XRD comparison of unmodified TiO_2 (red curve) and M-TiO_2 (black curve).

characteristic peaks of anatase TiO_2. In addition to the peaks that represent the regular anatase phase, the XRD survey of M-TiO_2 also shows a characteristic diffraction peak of the rutile phase of TiO_2 at a 2θ value of 27.5°.

Having some degree of rutile character along with the anatase phase could be advantageous as photo-induced electron transfer between rutile and anatase surface states in TiO_2 nanoparticles endows them with high surface photovoltage response and photocatalytic activity.[51] It should be noted that the intensity of the peak at 25° 2θ, corresponding to the diffraction from the (101) plane, is markedly enhanced for M-TiO_2 compared to unmodified TiO_2, which can be attributed to an increased crystallinity of the former compared to the latter sample. Studies suggest that increased crystallinity enhances the photocatalytic activity of TiO_2.[52−58] M-TiO_2 showcases an extra peak at 38° 2θ that corresponds to the (004) plane, which indicates that crystal growth mainly occurs along the [001] direction and that the {001} facets are exposed, a characteristic feature of anatase TiO_2 nanoparticles.[59] From the XRD data, an average particle size (D) of the samples was also calculated using the Debye−Scherrer formula. Using the formula, the average particle sizes of the TiO_2 particles were calculated to be 23 nm and that of M-TiO_2 particles was estimated to be 22.75 nm; these values are comparable to the particle sizes estimated from the transmission electron microscopy (TEM) data (*vide infra*). The relative contents of the anatase and rutile phases in the M-TiO_2 sample were calculated from the XRD intensity of the characteristic peaks of the phases[60] and were found to be 89.21% for anatase phase and 10.78% for rutile phase.

Fourier Transform Infrared Spectroscopy. Fourier transform infrared spectroscopy (FTIR) spectra of TiO_2, I-TiO_2, and M-TiO_2 were recorded[61] to analyze the modalities of surface modification on TiO_2, and are shown in Figure S1. The FTIR spectra of TiO_2, I-TiO_2, and M-TiO_2 appear to be largely similar with peaks that represent frequencies of stretching

https://doi.org/10.1021/acsomega.2c01425
ACS Omega 2022, 7, 25094−25109

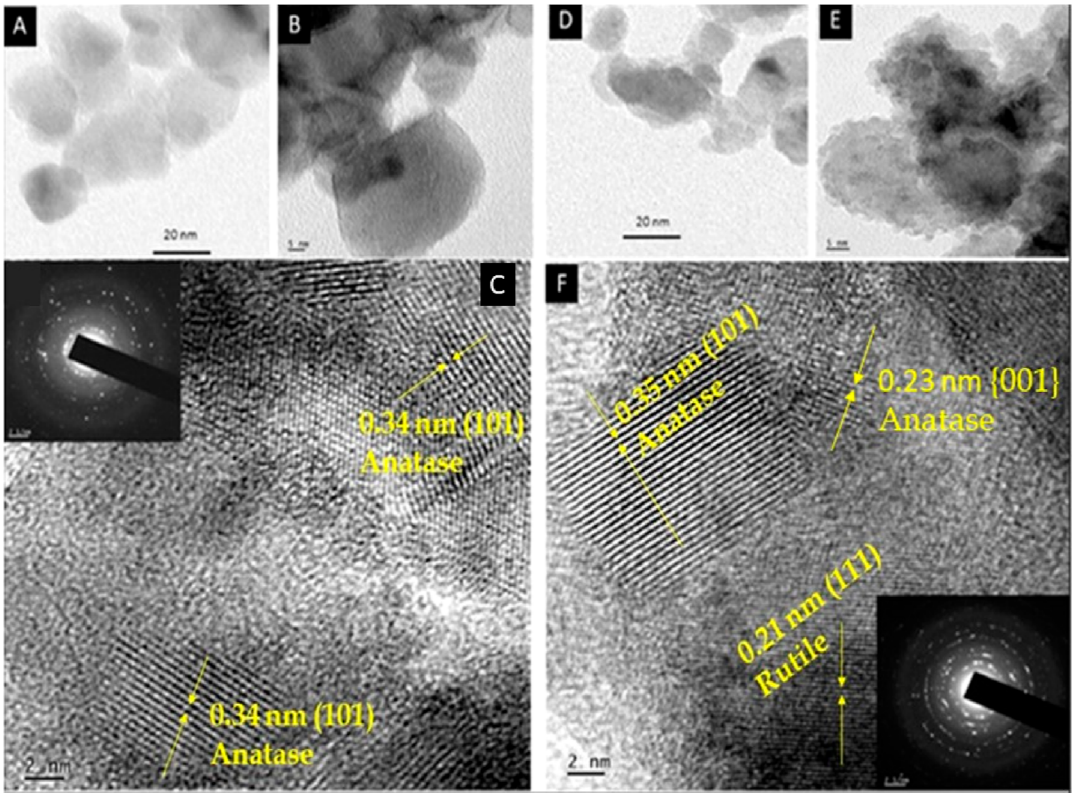

Figure 4. TEM images of TiO_2 (A–C) and M-TiO_2 (D–F). (A,B) TEM images of TiO_2 with different magnifications; (C) HRTEM image of TiO_2, and inset of (C) is the SAED pattern of TiO_2. (D,E) TEM images of M-TiO_2 with different magnifications, (F) HRTEM image of M-TiO_2, and inset of (F) is the SAED pattern of M-TiO_2.

(3500–3200 cm^{-1}) and bending (1700–1300 cm^{-1}) vibrations of O–H functional groups on the surface of TiO_2 nanoparticles and, possibly, of physisorbed water on TiO_2 surface and stretching (1300–1200 cm^{-1}) vibration of Ti–O–Ti bond system. The substantially weaker peak intensities of the O–H functional groups of M-TiO_2 compared to that of bare TiO_2, however, indicate that a significant fraction of the hydroxyl functional groups have reacted with the silane moieties. In addition, in contrast to the spectrum of unmodified TiO_2, I-TiO_2 and M-TiO_2 reveal a spectral feature at 1061 and 1045 cm^{-1} which can be ascribed to the Si–O bond stretching vibration.[62] The low-frequency band of I-TiO_2 at 940 cm^{-1} and that of M-TiO_2 at 932 cm^{-1} can be ascribed to the formation of Ti–O–Si bonds[63] in I-TiO_2 and M-TiO_2 by the interaction of the surface hydroxyl groups of TiO_2 with trimethyloxysilane. The intensity of these peaks is found to be reduced in M-TiO_2 compared to I-TiO_2; which can be attributed to the elimination of some silane groups from the surface of TiO_2 due to the double sintering process. Surprisingly, the photocatalytic performance of M-TiO_2 was found to be better than that of I-TiO_2 (*cf.* Figures S11 and S12), indicating that the double sintering process has resulted in just the optimal extent of surface functionalization required for better photocatalytic activity (*vide infra*). FTIR spectra of samples with different weight percentages of trimethoxy silane, such as TiO_2/trimethoxy silane of 0,1:1,1:2, 1:4, and 1:20 (Figure S2), were also compared to find the effect of modifier weight percentage change on the properties of the final product. Spectra showed all the peaks mentioned earlier such as frequencies of stretching (3500–3200 cm^{-1}) and bending (1700–1300 cm^{-1}) vibrations of O–H functional groups on the surface of TiO_2 nanoparticles and water on the TiO_2 surface and stretching (1300–1200 cm^{-1}) vibration of the Ti–O–Ti bond system. All the samples except sample 0, where silane is absent, showed the spectral feature of Si–O bond stretching vibration at ∼1060 and 1040 cm^{-1}. A trend showing an increase in the intensity of Si–O bond stretching vibration at ∼1060 cm^{-1} can be attributed to the change in trimethoxy silane weight percentage in the preparation of modified TiO_2. To assess the nature of the N-719 dye loading onto the TiO_2 nanoparticle surface, the FTIR spectra of TiO_2 and M-TiO_2 samples sensitized with the N-719 dye (same quantities of samples were scratched off from the photoanode films and were immersed in solutions of the N-719 dye[64] of same concentration for the same duration) were measured and are shown in Figure S3. The absorption peaks corresponding to components of N-719, such as thiocyanate group (–S–C≡N) (∼2100 cm^{-1}), carbonyl (∼1715 cm^{-1}), bipyridine (∼1545 cm^{-1}), tetrabutylammonium (TBA) counter-ions (∼1370 cm^{-1}), and carboxylic acid and carboxylate groups (∼3500–3000 cm^{-1}), were observed. It is apparent from the data that the intensities of the IR peaks of sensitized M-TiO_2 sample are greater than that of sensitized TiO_2, which indicates a greater extent of dye-loading on M-TiO_2 than bare TiO_2, evidently through a facile interaction, probably of hydrogen bonding in nature, between the carboxylic acid or carboxylate functional groups of the N-719 dye with Ti–O–Si bonds, and with free surface hydroxyl groups of TiO_2 nanoparticles.

Raman Spectroscopy. Raman spectra of TiO_2 and M-TiO_2 (Figure S4) were acquired to further probe how functionalization affects the properties of TiO_2. TiO_2 sample shows five characteristic Raman active modes of anatase TiO_2 at 140.11

https://doi.org/10.1021/acsomega.2c01425
ACS Omega 2022, 7, 25094–25109

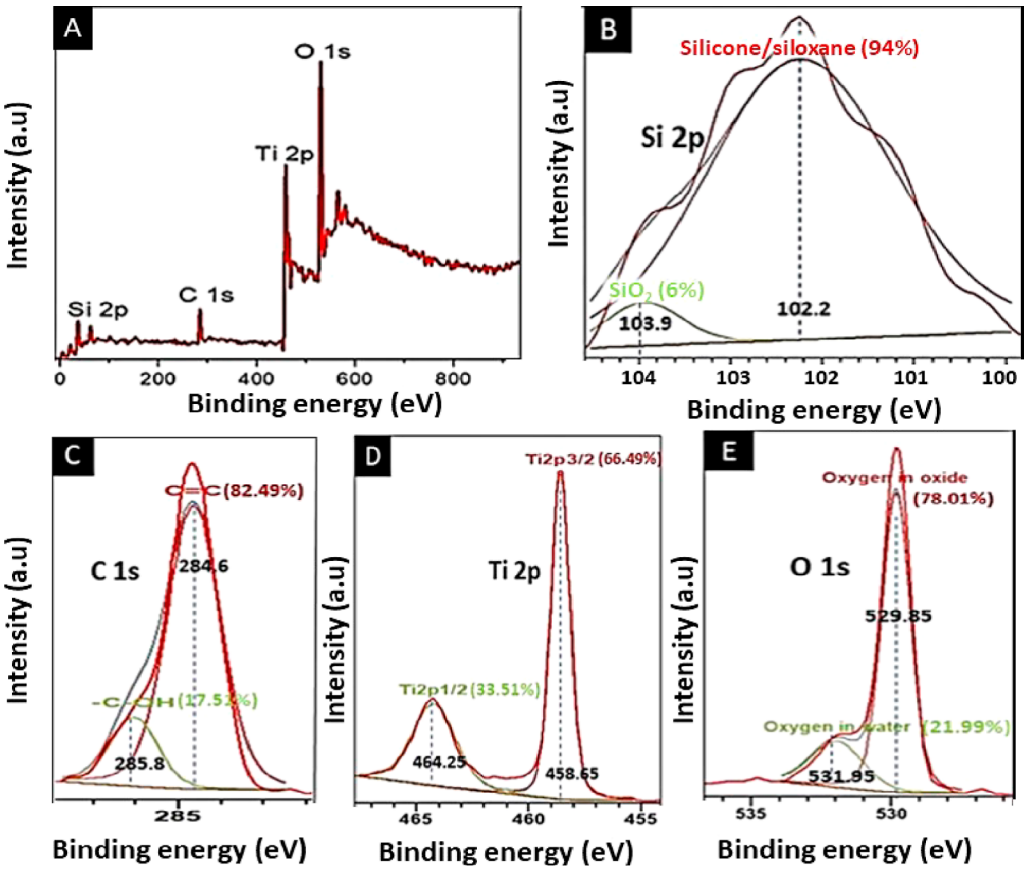

Figure 5. X-ray photoelectron spectroscopy (XPS) spectrum of M-TiO_2. (A) Wide spectrum, Core level spectra of (B) Si 2p, (C) C 1s, (D) Ti 2p, and (E) O 1s.

cm^{-1} (E_g), 196.4 cm^{-1} (E_g), 394.08 cm^{-1} (B_{1g}), 518.3 cm^{-1} (combination of A_{1g} and B_{1g} that cannot be resolved at room temperature), and 640.8 cm^{-1} (E_g).[65] All these peaks are due to vibrations of the O−Ti−O bonds, wherein, the vibrations of E_g symmetry are of symmetric stretching character, symmetric bending has a B_{1g} symmetry, and antisymmetric bending vibrations have an A_{1g} character. These characteristic vibrational frequencies and their intensity ratios confirmed the presence of phase pure anatase TiO_2. M-TiO_2 also exhibited similar characteristic peaks at 144.8, 394, 513.7, and 640.8 cm^{-1}, corresponding to vibrations of the O−Ti−O bonds. However, the intensity of the peak at 144.8 cm^{-1} is considerably diminished in the spectrum of M-TiO_2 compared to TiO_2; this can be attributed to the presence of rutile characteristics in it. In addition, compared to TiO_2, the A_{1g} + B_{1g} combination band of M-TiO_2 is found to be slightly shifted to lower energy; which can be ascribed to be due to the rutile characteristics[66] of M-TiO_2. A minute peak observed at 559.38 cm^{-1} can be assigned to the presence of silane moieties in the M-TiO_2 sample (magnified view of Figure S4).

Scanning Electron Microscopy. The scanning electron microscopy (SEM) images of TiO_2, I-TiO_2, and M-TiO_2, as shown in Figure S5A−C illustrate closely packed aggregates of grains having irregular and undefined shapes in all samples, however, surface modification in M-TiO_2 appears to increase aggregates size, resulting in a spongy appearance.

Transmission Electron Microscopy. TEM images of the prepared unmodified TiO_2[67] and modified M-TiO_2 are shown in Figure 4. From the TEM images, Figure 4A,B, it is clear that the size of the prepared TiO_2 nanoparticles is almost spherical and has dimensionalities in the range of 20−30 nm, a suitable range of particle size for optimum photocatalysis.[68] Figure 4C implies that TiO_2 shows the presence of only the anatase phase while M-TiO_2 shows both anatase and rutile phases. The inset of Figure 4C shows the SAED pattern of a single TiO_2 nanoparticle. From the high-resolution TEM (HRTEM) image (Figure 4C), a fringe width of 0.34 nm is deduced for the unmodified TiO_2 nanoparticles which correspond to the lattice parameter of the (101) plane of the anatase TiO_2. The SAED pattern further reveals that the unmodified TiO_2 nanoparticles are of polycrystalline nature. Figure 4D−F shows the TEM images of M-TiO_2 in the order of increased resolution, and these images also reveal a particle size range of 20−30 nm.

In comparison to the unmodified TiO_2 sample, M-TiO_2 has a porous structure which is shown in Figure 4E. The SAED pattern suggests a more polycrystalline nature of M-TiO_2, with a distribution of single crystals of M-TiO_2 in the matrix, which agrees very well with the XRD data. The lattice fringes observed in the HRTEM image suggest a fringe width of 0.23 nm, which can be ascribed to the exposed {001} facets of anatase TiO_2. The lattice fringes with 0.35 nm width suggest the (101) plane of anatase TiO_2, and the lattice fringe of 0.21 nm is attributed to the presence of the (111) plane of rutile TiO_2.[69] Of the several crystallographic planes exhibited by the anatase form of TiO_2, the (001) surface has been suggested to be the most reactive site for photocatalytic processes.[70] The TEM data suggests that the surface modification method has exposed the (001) facet of TiO_2, and the presence of a small percentage of the rutile phase makes M-TiO_2 a potential

https://doi.org/10.1021/acsomega.2c01425
ACS Omega 2022, 7, 25094−25109

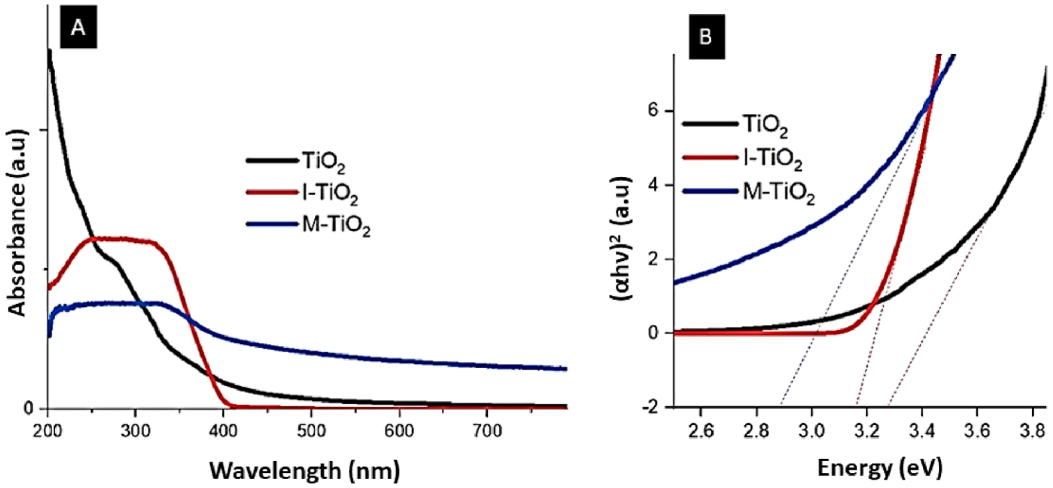

Figure 6. (A) Absorption spectra and (B) Tauc plot comparison of TiO_2, I-TiO_2, and M-TiO_2.

candidate in photocatalytic applications. TEM images of I-TiO_2 are shown in Figure S6. From the TEM images, Figure S6A,B, it is clear that the I-TiO_2 nanoparticles are also spherical in shape and have sizes in the range of 20−30 nm.

From the HRTEM image (Figure S6C), a fringe width of 0.34 nm is deduced for the unmodified TiO_2 nanoparticles which correspond to the lattice parameter of the (101) plane of the anatase TiO_2. Figure S6D shows the SAED pattern of I-TiO_2. The SAED pattern further reveals that the I-TiO_2 nanoparticles are also of polycrystalline nature.

Brunauer−Emmett−Teller Analysis. Brunauer−Emmett−Teller (BET) surface area analysis[71] was performed to study the surface area and porosity of the samples. The specific surface area of TiO_2 and M-TiO_2 was calculated using a BET plot and the surface area of M-TiO_2 was found to be 45.6454 m^2/g, and that of TiO_2 was found to be 30.684 m^2/g. This result indicates that surface modification has slightly improved the surface area of TiO_2, which is in contrast to the common trend that modification with silane moieties significantly reduces the surface area of TiO_2.[72]

The adsorption−desorption isotherm of TiO_2 and M-TiO_2 were plotted (Figure S7). TiO_2 shows a type II isotherm, typical of a nonporous or microporous adsorbent. The arrow point, the beginning of the almost linear middle section of the isotherm, is often taken to indicate the stage at which monolayer coverage is complete and multilayer adsorption is about to begin. From this data, the pore volume and pore diameter of TiO_2 was estimated to be 0.040603 cm^3/g and 5.2931 nm, respectively. M-TiO_2, however, belongs to a type IV classification, featuring a hysteresis loop, associated with capillary condensation in the mesopores, and a limited nitrogen uptake over a range of high (P/P_o). The initial part of the isotherm is attributed to a monolayer coverage. The pore volume and pore diameter of M-TiO_2 was found to be 0.124887 cm^3/g and 9.53764 nm, respectively. These results confirm that both the surface area and the porosity of TiO_2 have increased upon surface modification.

Energy-Dispersive X-ray Spectroscopy. Energy-dispersive X-ray spectroscopy (EDX) spectra of TiO_2 and M-TiO_2 were taken to analyze their elemental compositions (Figure S8). The data revealed that TiO_2 consists of 61.47% Ti and 27.85% O, whereas M-TiO_2 is composed of 62.29% Ti and 33.22% O. A noteworthy observation from the EDX spectrum of M-TiO_2 is that it contains 4.49% of Si; this, when taken together with data presented *vide supra*, confirms that the silane groups are functionalized onto the TiO_2 surface.

X-ray Photoelectron Spectroscopy. XPS is a commonly used technique[73] to determine the valence band maximum (VBM) in a semiconductor (Figure S9). The VBM of the prepared M-TiO_2 sample was determined by a linear extrapolation method and found to be 0.88 eV. Combining the band gap value obtained from the Tauc plot (*vide infra*) with this result, the conduction band minimum[74] can be estimated to be around −2.05 eV. The XPS spectrum (Figure 5A) of the M-TiO_2 sample showed characteristic peaks corresponding to Si 2p, C 1s, Ti 2p, and O 1s at 102, 285, 458, and 530 eV respectively. The fitted curve for the same gives an idea about the mass concentrations of these elements. Mass concentrations are as follows: Si 2p—14.96%, C 1s—41.42%, Ti 2p—39.82%, and O 1s—3.8%. Figure 5B demonstrates the core level spectrum[75] of Si 2p,[76] which can be resolved into contributions of silicone/siloxane (94%) and SiO_2 (6%). In Figure 5C, a core level spectrum of C 1s of the M-TiO_2 sample reveals a peak pattern at 285 eV, which can be further resolved into two peaks: one at 284.6 eV, due to sp^2-hybridized carbon atoms (82.49%), and another one at 285.8 eV, due to carbons that are bound to an −OH group (17.51%) present in the composite.[77] Figure 5D illustrates the core level spectrum of Ti 2p (458 eV) with peaks resolved at 458.65 and 464.25 eV, corresponding to Ti $2p_{3/2}$ (66.49%) and Ti $2p_{1/2}$ (33.51%), respectively. Figure 5E illustrates the core level spectrum of O 1s, wherein, peak fitting resulted in two peaks, the first one at 529.85 eV, which can be assigned to reticular O in the oxide (78.01%), and a second one at 531.95 eV, which can be attributed to oxygen in the surface water (21.99%) molecules.

UV−Visible Spectroscopy and Band Gap Determination. UV−visible spectroscopy was carried out to compare the absorbance spectra of TiO_2, I-TiO_2, and M-TiO_2 and is shown in Figure 6A. The absorption spectrum of M-TiO_2 is significantly redshifted than that of TiO_2 and I-TiO_2, indicating a larger fraction of the rutile phase in M-TiO_2 and an appreciable reduction of the bandwidth of the M-TiO_2. The optical band gap of thin films of TiO_2, I-TiO_2, and M-TiO_2 was calculated using Tauc's equation. Figure 6B shows the Tauc plot obtained from the optical absorption spectra. Tauc plot reveals a band gap of 3.27 eV for TiO_2, 3.15 eV for I-TiO_2, and 2.93 eV for M-TiO_2, confirming that the band gap decreases

https://doi.org/10.1021/acsomega.2c01425
ACS Omega 2022, 7, 25094−25109

upon surface modification of TIO_2; an effect that can be due to the presence of the rutile phase in M-TiO_2.[78] The conduction band of the rutile phase of TiO_2 lies higher than that of the anatase phase. A hierarchical arrangement of the conduction bands could render an effective transfer of the photo-generated electrons of the exciton pair from the rutile phase to the lattice trapping sites of the anatase phase. This could inhibit the electron−hole recombination in the rutile phase and result in the effective separation of the photogenerated electron−hole pair. In photocatalytic applications, this ensures that the electrons reach the pollutant surface, and makes the photocatalysis more effective (*cf.* Figure S10). In the case of DSSC applications (Figure S11), effective separation of the electron−hole pair among the rutile and anatase phases could facilitate easy transfer of the electrons from the anatase phase to a transparent conducting electrode and boost the efficiency of the device.[79] UV−visible spectroscopy was carried out to compare the absorbance spectra of samples with different relative ratios weight percentages of trimethoxy silane with respect to TiO_2 *viz.* 0, 1:1, 1:2, 1:4, and 1:20. Figure S12 shows the absorption spectra and corresponding Tauc plots of all the combinations. Figure S12A shows the absorption spectra of all the samples. The absorption spectrum of the 1:2 sample (M-TiO_2) is significantly redshifted than that of other samples. The optical band gaps of the samples were calculated using Tauc's equation. Figure S12B shows the Tauc plot obtained from the optical absorption spectra. Tauc plots revealed band gaps of 3.27, 3.11, 2.93, 3.10, and 3.20 eV for 0, 1:1, 1:2, 1:4, 1:20 samples, respectively. The 1:2 sample (M-TiO_2) showed the narrowest band gap and has the maximum coefficient of absorption. These data unequivocally illustrate that surface modification has caused a redshift in the absorption wavelength till the extent of optimum modification, after which, a blueshift in the absorption maximum was observed.

Photoluminescence Spectroscopy. Photoluminescence spectroscopy (PL) gives a hint about the recombination of photo-generated excitons, where the intensity of PL spectra reveals the recombination rate; indicating that the low intensity of the PL represents a low recombination rate of photo-generated carriers. The presence of defect-related excitation peaks can be analyzed effectively by observing the PL spectra. PL spectra of TiO_2, I-TiO_2, and M-TiO_2 were obtained by exciting the samples at a wavelength of 320 nm, and are shown in Figure S13. M-TiO_2 exhibits a weaker PL emission intensity than that of I-TiO_2 and TiO_2 indicating that exciton recombination is more retarded in M-TiO_2 than in others. Nonradiative recombination mostly occurs on the grain boundary; double sintering done during the M-TiO_2 sample preparation stage effectively removes these boundaries and nonradiative defects, thus retarding the nonradiative recombination processes, which makes M-TiO_2 a better candidate for photocatalytic and photovoltaic applications.[67] In addition to this, different band alignments at the interface between anatase and rutile phases in M-TiO_2 also separate the excitons from recombination. It can also be reasonably envisaged that surface modification with optimum silane concentration could decrease the number of oxygen defects. The low intensity of PL emission is attributed to the hopping of electrons through small neighboring defect sites until it finds a recombination center. PL spectra of samples with different ratios of weight percentages of trimethoxy silane and TiO_2 (0,1:1,1:2, 1:4, and 1:20) were compared and shown in Figure S14. When silane concentration increases, PL emission was found to decrease. However, after a point, when the concentration continues to increase, PL also concomitantly increases. Reduction in recombination sites upon modification with silane reduces the PL intensity but once the optimum silane concentration has passed, with increasing concentration of silane, silane moieties hinder the charge carriers, causing faster recombination. Among the 5 graphs, sample 1:2 shows the least value for the PL emission. PL spectra were composed of mainly two peaks, one at ∼420 nm, indicating band-edge free exciton luminescence, and the other at ∼470 nm, indicating bound exciton luminescence caused by the defect of the oxygen hole on the sample surface.[80,81] The ratio of the intensities of the peaks at 470 to 420 nm is shown in Table. S1. The ratio tends to decrease as the silane concentration increases up to an optimum level and then tends to increase. The least ratio was deduced for sample 1:2 which indicates a greater number of band-edge free excitons in sample 1:2 and, hence, better photocatalytic activity.

Time-Correlated Single-Photon Counting. Time-correlated single-photon counting (TCSPC) is a well-known technique for fluorescence lifetime measurements.[82] TCSPC detects single photons and measures their arrival time with respect to a reference signal, usually, the light source used. Using TCSPC, information about energy transfer, electron/hole transfer, indirect information about trap states (both surface traps and intrinsic traps), and a plethora of other properties of electronics excited states can be deduced. TCSPC measurement of samples with different weight percentages of trimethoxy silane (TiO_2/trimethoxy silane as 0,1:1,1:2, 1:4, and 1:20), and the same samples mixed with the MB dye was compared to obtain a clear picture about the charge carrier transport inside the material (Figure S15). Sample 1:2 demonstrated the maximum lifetime while sample 0 got the least value. Factors such as the number of trap sites and the band structure of the material can influence the charge carrier lifetime of the material. Vacancies tend to be more in the unmodified form of TiO_2 because the carriers trapped in a defect center cannot directly jump to the valence band. Electron hopping from one defect site to another becomes difficult because the electron finds a number of radiative centers along its path. However, in modified TiO_2, the electron can travel a long way before finding a radiative center because the electrons are relaxed for a longer period.

Modified TiO_2 consists of an anatase-rutile mixed-phase, wherein band bending at the interface between the anatase and the rutile occurs due to the conduction band edge difference (∼0.2 eV) between the two phases. The electron transfer occurs from the conduction band of anatase to the conduction band of rutile, and thus, due to band bending, the charge carriers are effectively separated. Charge carriers will have a long life when the anatase phase and rutile phase are in contact with each other. Apart from this, the nonradiative centers at the interface also act as shallow trap centers preventing the direct transition of electrons from the conduction band of anatase to that of rutile, and therefore, the electrons take a longer time to move from the anatase conduction band to a rutile conduction band.

Cross-Cut Adhesion Test. An adhesion test of the M-TiO_2 sheet was done using a cross-cut test.[83] The result observed is shown in Figure S16. The cut area of the test coating was examined by visual comparison with the illustrations in the standard (ISO 2409), depending on the amount of flaked coating. Edges of the cuts were smooth with a detachment of

https://doi.org/10.1021/acsomega.2c01425
ACS Omega 2022, 7, 25094−25109

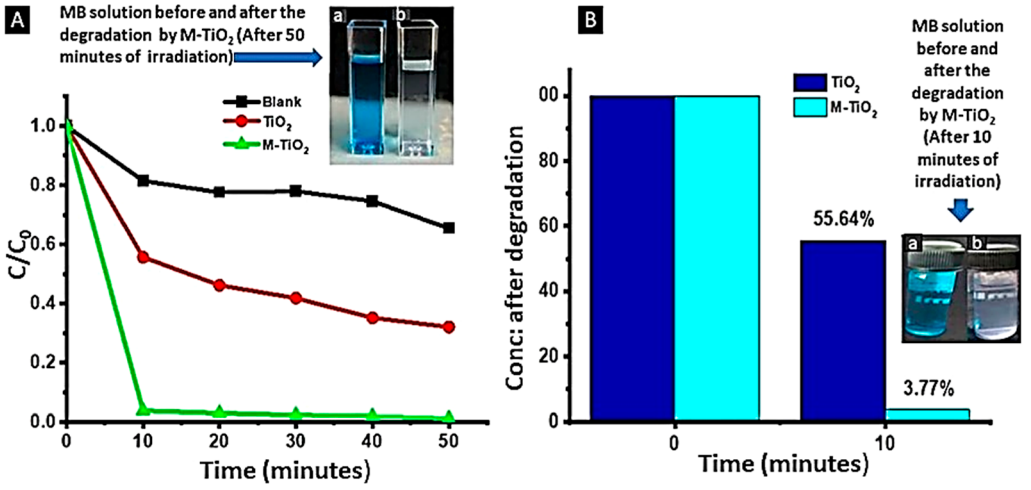

Figure 7. (A) C/C_0 *vs* Time graph of TiO_2 and M-TiO_2, (B) percentage of degradation of the same after 10 min of irradiation.

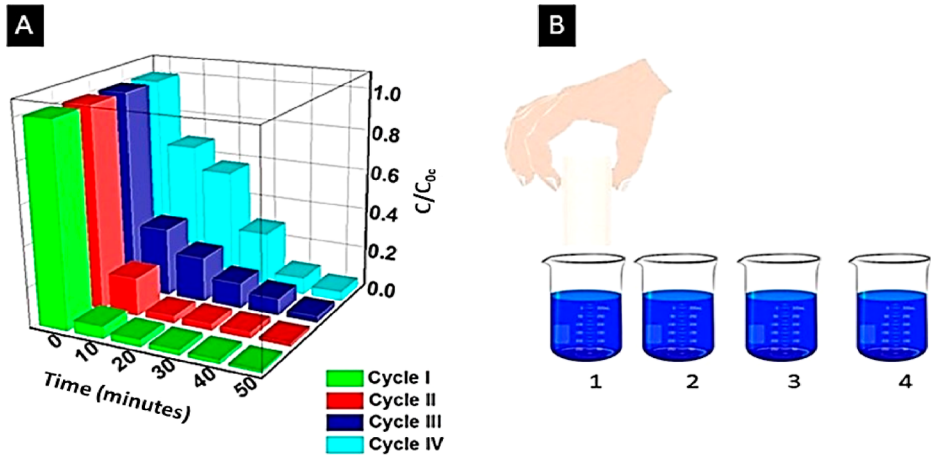

Figure 8. (A) C/C_0 *vs* time graph of M-TiO_2 for four consecutive cycles and (B) pictorial representation of recycling using a flexible M-TiO_2 sheet.

less than 5% flakes from the coating, and the coating was classified as 1 according to the standard.

Evaluation of Photocatalytic Activity for the Use in Wastewater Treatment. *UV–Visible Spectroscopy.* To explore the photocatalytic activity of synthesized M-TiO_2, photocatalytic degradation of MB was attempted because MB is a notable water pollutant, carcinogenic and mutagenic, and is a well-established dye used in numerous photocatalytic studies. The standard photocatalytic mechanism[69] involves the formation of electron–hole pairs in photoexcited TiO_2; the holes oxidize the surface hydroxide ions or water molecules of TiO_2 into hydroxyl radicals ($OH^{\bullet}$), and electrons react with oxygen to form superoxide radical anions ($O_2^{\bullet -}$) which, if abstract protons from the aqueous media, may form hydroperoxyl radicals (HOO^-). The photoexcited MB, on the other hand, may inject electrons into the conduction band of TiO_2 to form a radical cation, which reacts with $OH^{\bullet}$ to form the organic degradation products. Figure S17 showcase the absorption spectra of TiO_2, I-TiO_2, and M-TiO_2 taken at different time intervals. The rate of degradation was recorded with respect to the changes in the intensity of absorption peak in the visible region where monomeric MB exhibits the (0–0) and (0–1) vibronic features at ~664 and ~610 nm, respectively.[84] It can be visualized that as irradiation time increases, the intensity of the absorption peaks of monomeric MB decreases. Figure 7A shows the graph of concentration reduction of MB taken in an aqueous solution containing bare TiO_2 and M-TiO_2 without any photocatalyst as a function of time (labeled as blank). The inset of Figure 7A(a,b) shows the photographs of MB solution in the presence of the M-TiO_2 catalyst before and after degradation (after 50 min of irradiation). M-TiO_2 showed 99.98% of degradation after 50 min of irradiation, whereas TiO_2 showed only 68.01% degradation after 50 min of irradiation. It should be mentioned that I-TiO_2 showed an intermediate efficiency of dye-degradation, that is, 81.37% degradation after 50 min of irradiation. The inset of Figure 7B shows the degraded MB solutions with TiO_2 (a) and M-TiO_2 (b) after 10 min of starting the irradiation. A comparative study of the photocatalytic activity of TiO_2, I-TiO_2, and M-TiO_2 is shown in Figure S18. (C/C_0) *versus* time graph of TiO_2 and M-TiO_2 samples is shown in Figure S18A, and the percentage of degradation of TiO_2 and M-TiO_2 samples with respect to time is shown in Figure S18B. Our photocatalysis results indicate that M-TiO_2 is better than bare TiO_2 and I-TiO_2 in accelerating the degradation of MB. We attribute the better performance of M-TiO_2 (color of the MB solution vanishes after 50 min of degradation using M-TiO_2 as in Figure S19) to the following reasons: (i) silanization could have made the surface of TiO_2 more hydrophobic,[85] which could facilitate

https://doi.org/10.1021/acsomega.2c01425
ACS Omega 2022, 7, 25094–25109

better interaction of the surface with nonpolar parts of MB, an effect that is unlikely to occur between MB and the superhydrophilic surface (due to the decomposing adsorbed organic residues) of bare TiO_2, and (ii) the most reactive {001} facets of TiO_2 is exposed upon silanization, which possibly could have promoted the rate of photocatalytic degradation of MB. In order for M-TiO_2 to be used as a catalyst in practical applications, its reusability after every photocatalytic application event must be checked. Figure 8A shows that even at the end of the fourth consecutive cycle of photocatalysis, M-TiO_2 is capable of degrading 95.44% of MB in an aqueous solution after 50 min of irradiation time; a performance that is still far superior compared to the performances of TiO_2 and I-TiO_2. A disadvantage of using conventional recyclable photocatalysts in powder form is that after every photocatalytic cycle, the solution needs to be centrifuged to recover the catalyst. Herein, the flexible M-TiO_2 sheets dipped into the dye solution can be just lifted off once the photocatalysis is completed with negligible loss of photocatalyst from the sheet; implying that M-TiO_2 sheets should be able to retain their performance over a number of catalysis cycles (Figure 8B).

Role of the Silane Content on the Performance of the Photocatalyst. For a better understanding of the high photocatalytic dye degradation efficiency of M-TiO_2, 5 samples with different silane contents with respect to the TiO_2 content (labeled 0:1,1:1,1:2, 1:4, and 1:20) were analyzed, and photocatalytic dye degradation efficiencies were compared. Figure S20 shows the (C/C_0) *versus* time graph of M-TiO_2 with different silane contents. Bare TiO_2 showed a dye degradation of 68.01% after 50 min of irradiation, which was the lowest among the five. The incorporation of silane increased the dye degradation drastically (96.25%) for the 1:1 sample. 1:2 sample showed a remarkable dye degradation of 99.98%. The 1:4 sample, however, showed a decrease in performance (98.50%) and 1:5 showed a further decrease (97.87%). From the graph, it can be perceived that the presence of silane plays a crucial role in the photocatalytic performance of TiO_2. An optimum level of silane weight percentage in the modified photocatalyst favors the dye degradation efficiency because the presence of silane endows better adhesion between each TiO_2 particle as well as between the particles and the substrate. This enables a crack-free surface and lowers the number of trap sites and recombination and improves the charge transport. The correct length of the ligand chain connecting two TiO_2 particles increases the pathway of electron transport and reduces recombination. When the nonconducting silane content exceeds a limit, it affects the conductivity and acts as a barrier to electron transport, causing a reduction in dye degradation efficiency.

Scavenger Study. A scavenger study[86] was performed to find out the active radicals responsible for the photodegradation activity of TiO_2 and M-TiO_2 and to elucidate the mechanism of photocatalysis. Scavengers are species that undergo a fast reaction specifically with a radical, generate a stable species that does not interfere with the reaction, erase the effect of radical in the degradation process, and help examine the nature and role of oxidative species involved in the photocatalytic reaction. IPA was used as a hydroxyl radical scavenger, silver nitrate ($AgNO_3$) was applied as an electron scavenger, and EDTA was used as a hole scavenger. Figure S21 shows the effect of the scavengers on the photocatalytic activity of TiO_2 and M-TiO_2 samples. In the case of the TiO_2 sample, within the first 10 min of irradiation, the addition of IPA, $AgNO_3$, and EDTA diminished the photocatalytic activity to 40.21, 58.13, and 68.26% respectively. The apparently greater reduction in the rate of photocatalytic degradation upon adding IPA indicates that $^{\bullet}OH$ radicals are the prime active species responsible for the oxidation of unmodified TiO_2, consistent with the previous reports.[87] When the scavenger study was done for M-TiO_2, adding $AgNO_3$ resulted in a minimum degradation rate (48.42%) than that of IPA (52.67%) and EDTA (67.06%), indicating that electron is the active species responsible for the catalytic activity.

Modification of TiO_2 with silane moieties changed the active species responsible for the photocatalytic activity, presumably due to the mixed anatase/rutile nature of M-TiO_2 and due to excess electrons present in modified TiO_2.

Evaluation of Photovoltaic Properties for Use in DSSC. *UV−Visible Spectroscopy.* The extent of N-719 dye loading on TiO_2 and M-TiO_2 was evaluated by recording the UV−visible absorption spectrum of both TiO_2 and M-TiO_2 of the same quantities (scratched-off from the photoanode films) soaked in the dye for the same duration and under identical experimental conditions and are shown in Figure S22. The absorption profiles of both TiO_2 + N-719 and M-TiO_2 + N-719 show the characteristic peaks of N-719 at *ca.* 390 and 530 nm. However, the absorption peak of the M-TiO_2 + N-719 sample at 530 nm exhibits an enhanced intensity and a slight red-shift (536.5 nm) compared to the TiO_2 + N-719 sample, implying an enhanced dye-adsorption on the surface of M-TiO_2; in agreement with the FT-IR data.

Photochronoamperometry. The photocurrent densities of TiO_2 and M-TiO_2 were compared[88] using photochronoamperometry measurements carried out at a constant voltage of 0.5 V, and under light and dark conditions, and are illustrated in Figure 9. From the graph, it can be observed that when

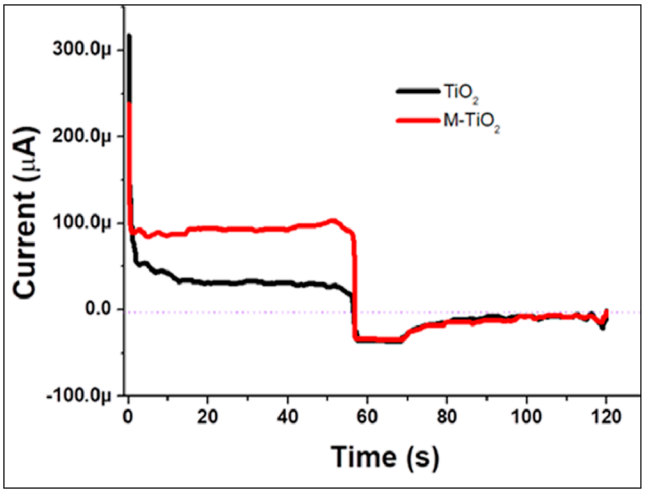

Figure 9. Photo chronoamperometry curve comparison of N719 dye-adsorbed TiO_2 and M-TiO_2.

illuminated with sunlight, the M-TiO_2 + N-719 sample has shown more current density than the TiO_2 + N-719 sample. In dark conditions, both samples give the same magnitudes of current densities.

Electrochemical Impedance Spectroscopy. EIS is a powerful tool to examine the characteristic properties of the electrode material such as resistance, impedance, and charge transfer.[89] For EIS experiments, the electrodes were immersed

https://doi.org/10.1021/acsomega.2c01425
ACS Omega 2022, 7, 25094−25109

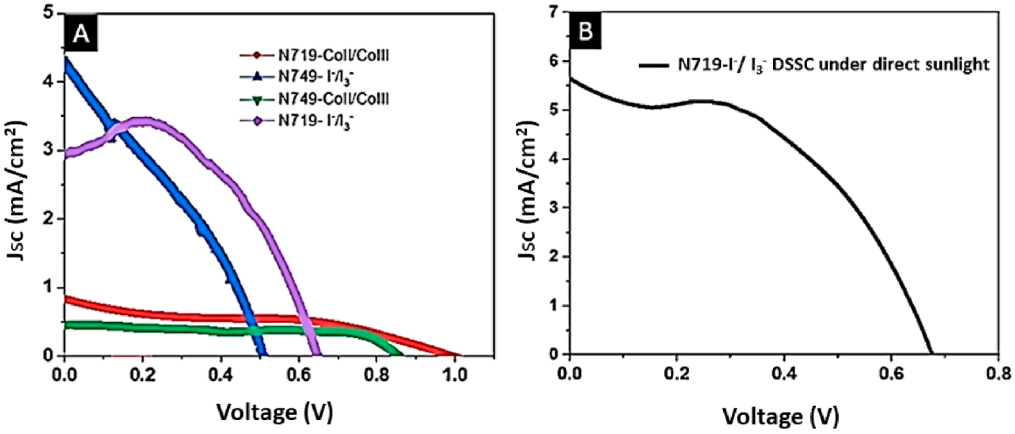

Figure 10. (A) *IV* characteristics of DSSCs measured with different electrolyte and dye combinations under AM 1.5 light conditions (B) *I*−*V* measurement of the best-performing device (N719−I_3^-/I^-) measured under direct sunlight conditions (with a device structure of ITO-N719 dye-adsorbed TiO_2 photoanode−I_3^-/I^- electrolyte−Pt counter electrode).

in (I^-/I_3^-) electrolyte−acetonitrile mixture for 1 h, and the measurements were taken under visible light. Figure S23 shows the EIS spectra of electrodes of TiO_2 and M-TiO_2. We attribute the enhancement in the photovoltaic properties of M-TiO_2 to the enhanced hydrophobic nature of the nanoparticle surface rendered by the silanization process that offers better interaction with the nonpolar parts of the dye and retarded back electron transfer and charge recombination processes at semiconductor/electrolyte interfaces. EIS spectra of DSSCs with TiO_2 and M-TiO_2 as photoanodes, N719 dye as the photosensitizer, and I_3^-/I^- redox couple as the electrolyte were compared. To have an insight into the resistance developed at the interfaces of different components of the DSSCs, impedance curves were analyzed, the impedance data were plotted as a Nyquist diagram (Figure S24), and the fit and simulation processes were achieved using the Z-fit tool provided in the EIS spectroscopy package. From the fitted curves of Nyquist plots, and the equivalent circuit, values of resistances and capacitances formed at the interfaces of DSSCs were determined. From the values of R_{ct} and C obtained from the EIS spectra, recombination lifetimes can be calculated (Figure S25). Table S2 shows the values of R_s, R_{CE}, R_{ct}, C_{CE}, and C of the DSSCs employing TiO_2 and M-TiO_2 as photoanodes.

The electron recombination in the photoanode−electrolyte interface is dependent on the recombination lifetime (τ_{oc}) and is calculated by eq 1.

$$\tau_{oc} = R_{ct}C \quad (1)$$

Where R_{ct} is the charge transfer resistance and C is the capacitance of the photoanode−electrolyte interface. From the data, it was estimated that the recombination lifetime of the device containing M-TiO_2 (6.7 ms) is greater than that of the device containing TiO_2 (5.02 ms). This proves that the carriers recombine 1.33 times faster in DSSC with TiO_2 than in that with M-TiO_2.

I−*V Measurements.* In order to illustrate the applicability of the prepared M-TiO_2 in photovoltaics, DSSCs with combinations of two different dyes, and electrolytes were fabricated using M-TiO_2 as the anode and platinum as the counter electrode, and the *I*−*V* characteristics of four types of DSSCs were compared *viz.* DSSC with N749 dye−I_3^-/I^- electrolyte (N749−I_3^-/I^-), N749 dye−Co(II)/Co(III) electrolyte (N749−Co(II)/Co(III)), N719 dye−I_3^-/I^- electrolyte (N719−I_3^-/I^-), and N719−Co(II)/Co(III) electrolyte (N719−Co(II)/Co(III) under AM 1.5 light conditions (Figure 10A). The input power of the light source was calibrated using a polycrystalline silicon reference solar cell. The device was exposed to direct sunlight with a power of 536 W/m^2 with a latitude of 9.669090, a longitude of 76.539070, and an elevation of 21 m. Under these conditions, the *J*−*V* characteristics of the device were measured using a potentiostat SP-200 (Biologic) supported by EC-Lab software and is shown in Figure 10A. The results are summarized in Table 2.

Table 2. *I*−*V* Measurement Results Comparison of DSSCs

DSSC	J_{sc} (mA/cm^2)	fill-factor	V_{oc} (V)	η (%)
N749−I_3^-/I^-	4.4	0.31	0.50	0.7
N749−Co(II)/Co(III)	0.5	0.67	0.82	0.28
N719−I_3^-/I^-	3.0	0.58	0.63	1.1
N719−Co(II)/Co(III)	0.8	0.46	1.02	0.41

It is evident that N719−I_3^-/I^- DSSC exhibits the highest efficiency (average value of several measurements) among all the tested devices (Figure 10B) under direct sunlight, and a short-circuit photocurrent density of 5.6 mA/cm^2, an open-circuit voltage of 0.68 V and a fill factor of 0.58 was obtained, and the photoconversion efficiency was found to be 4.1%. The value of photoconversion efficiency is less because of the low-lying conduction band of the ITO sheet used for the DSSC fabrication. A judicious selection of components of DSSC can improve efficiency. Sewvandi *et al.* have reported[62] high-performance DSSCs made of the N719 dye and TiO_2 electrodes having their surface modified with hydrocarbon and fluorocarbon silanes of varying chain lengths. They attributed the high efficiency of the DSSCs to the formation of a monolayer of the silane on the TiO_2 surface that prevents back electron transfer from TiO_2 to the I_3^- species; thereby, making the injected electrons available to perform the electrical work in the device. Our results indicate that surface modification of TiO_2 with silanes increases its photocurrent density and enhances the charge-separation efficiency when being employed in a photoanode scheme, which underlines the scope of using M-TiO_2 type materials to boost the efficiency of DSSCs.

https://doi.org/10.1021/acsomega.2c01425
ACS Omega 2022, 7, 25094−25109

CONCLUSIONS

Herein, we describe the synthesis, characterization, photophysical and electrochemical studies of TiO_2 nanoparticles surface modified with trimethyloxy silane functional groups. The prepared M-TiO_2 particles contain both rutile and anatase phases, with the {001} facets of them exposed by silanization. Flexible sheets of M-TiO_2 are prepared on a plastic substrate with a simple, scalable, and low-cost method and are used in a photocatalytic scheme and as a photoanode for DSSC applications. Based on the photocatalytic experiments, M-TiO_2 sheets outperform sheets made of unmodified TiO_2 nanoparticles in degrading the MB dye. Also, compared to unmodified TiO_2, M-TiO_2 sheets exhibited greater magnitudes of photocurrent when sensitized with the N-719 dye, and DSSC fabricated using M-TiO_2 as the photoanode exhibited a photoconversion efficiency of 4.1% under direct sunlight. These two effects could be attributed to (i) better interaction between the hydrophobic surface of M-TiO_2 with the nonpolar parts of the structure of the dye, facilitating better charge transport between the duo; (ii) co-existence of both rutile and anatase phases of TiO_2 and photo-induced electron transfer between them; (iii) formation of silane monolayer on the surface of TiO_2 which retards the back electron transfer from TiO_2 to the redox electrolyte or dye; and (iv) the formation of exposed {001} facets of TiO_2 upon surface modification, which confine the photo-generated excitons in the case of anatase TiO_2, and thus are endowed with a pronounced photoelectrochemical activity.

ASSOCIATED CONTENT

Supporting Information

The Supporting Information is available free of charge at https://pubs.acs.org/doi/10.1021/acsomega.2c01425.

Materials and Methods, Characterization techniques, Detailed results, FTIR spectra, Raman spectroscopy, SEM and TEM images, BET isotherms, EDX spectra, valence band maximum, mechanism of electron-hole separation, PL spectra, TCSPC measurement, Photographs, Absorption spectra, scavenger study, and EIS spectra (PDF)

Video of the photocatalytic degradation of MB using M-TiO_2 flexible sheet. (MP4)

Video displaying the M-TiO_2-applied ITO-coated PET flexible sheet (MP4)

AUTHOR INFORMATION

Corresponding Author

Suresh Mathew − *Advanced Molecular Materials Research Centre, Mahatma Gandhi University, Kottayam 686 560 Kerala, India; School of Chemical Sciences, Mahatma Gandhi University, Kottayam 686 560 Kerala, India;* orcid.org/0000-0002-7461-3438; Email: sureshmathewmgu@gmail.com

Authors

Soorya Sasi − *Advanced Molecular Materials Research Centre, Mahatma Gandhi University, Kottayam 686 560 Kerala, India*

Akash Chandran − *School of Chemical Sciences, Mahatma Gandhi University, Kottayam 686 560 Kerala, India*

Sunish K. Sugunan − *Department of Chemistry, CMS College Kottayam (Autonomous)—affiliated to Mahatma Gandhi University, Kottayam 686001 Kerala, India;* orcid.org/0000-0003-4104-2058

Ardra C Krishna − *School of Chemical Sciences, Mahatma Gandhi University, Kottayam 686 560 Kerala, India*

Pankajakshan Radhakrishnan Nair − *Advanced Molecular Materials Research Centre, Mahatma Gandhi University, Kottayam 686 560 Kerala, India*

Aneena Peter − *School of Chemical Sciences, Mahatma Gandhi University, Kottayam 686 560 Kerala, India*

Arsha N. Shaji − *School of Chemical Sciences, Mahatma Gandhi University, Kottayam 686 560 Kerala, India*

Kavasseri. R. V. Subramanian − *Department of Mechanical Engineering, Ramaiah Institute of Technology, Bangalore 560054, India;* orcid.org/0000-0002-8809-1992

Narendra Pai − *School of Chemistry, Monash University, Clayton, Victoria 3800, Australia;* orcid.org/0000-0003-1053-8827

Complete contact information is available at: https://pubs.acs.org/10.1021/acsomega.2c01425

Author Contributions

The manuscript was written through the contributions of all authors. All authors have given approval to the final version of the manuscript.

Notes

The authors declare no competing financial interest.

ACKNOWLEDGMENTS

This work was supported by Advanced Molecular Materials Research Centre, Mahatma Gandhi University, Kottayam-686 560, Kerala, India. We acknowledge Bhagyalakshmi Balan, Namitha N. N., and Sreerenjini C.R for their technical assistance.

ABBREVIATIONS

DSSC, dye-sensitized solar cell; HRTEM, high-resolution TEM; I-TiO_2, intermediate TiO_2; ITO, indium tin oxide; MB, methylene blue; M-TiO_2, modified TiO_2; PET, polyethylene terephthalate

REFERENCES

(1) (a) Zhou, T.-T.; Zhao, F.-H.; Cui, Y.-Q.; Chen, L.-X.; Yan, J.-S.; Wang, X.-X.; Long, Y.-Z. Flexible TiO_2/PVDF/g-C_3N_4 Nanocomposite with Excellent Light Photocatalytic Performance. *Polymers* **2020**, *12*, 55−69. (b) Thirunavukkarasu, G. K.; Monfort, O.; Motola, M.; Motlochová, M.; Gregor, M.; Roch, T.; Čaplovicová, M.; Lavrikova, A. Y.; Hensel, K.; Brezová, V.; Jerigová, M.; Šubrt, J.; Plesch, G. Ce ion surface-modified TiO_2 aerogel powders: a comprehensive study of their excellent photocatalytic efficiency in organic pollutant removal. *New J. Chem.* **2021**, *45*, 4174−4184. (c) Fadli, M. H.; Ibadurrohman, M.; Slamet, S. Microplastic Pollutant Degradation in Water Using Modified TiO_2 Photocatalyst Under UV-Irradiation. *IOP Conference Series: Materials Science and Engineering*; IOP Publishing, 2021; Vol. *1011*, p 012055.

(2) (a) Chen, D.; Huang, F.; Cheng, Y.-B.; Caruso, R. A. Mesoporous Anatase TiO_2 Beads with High Surface Areas and Controllable Pore Sizes: A Superior Candidate for High-Performance Dye-Sensitized Solar Cells. *J. Adv. Mater.* **2009**, *21*, 2206−2210. (b) Chou, J.-C.; Lin, Y.-C.; Lai, C.-H.; Kuo, P.-Y.; Nien, Y.-H.; Chang, J.-X.; Hu, G.-M.; Yong, Z.-R. Electron Conduction Channel of Silver Nanowire Modified TiO_2 Photoanode for Improvement of Interface Impedance of Dye-Sensitized Solar Cell. *IEEE J. Electron Devices Soc.* **2021**, *9*, 250−256.

(3) Baldini, E.; Palmieri, T.; Dominguez, A.; Rubio, A.; Chergui, M. Giant Exciton Mott Density in Anatase TiO_2. *Phys. Rev. Lett.* **2020**, *125*, 116403.
(4) Park, N.-G.; Van de Lagemaat, J.; Frank, A. J. Comparison of Dye-Sensitized Rutile- and Anatase-Based TiO_2 Solar Cells. *J. Phys. Chem. B* **2000**, *104*, 8989−8994.
(5) Luttrell, T.; Halpegamage, S.; Tao, J.; Kramer, A.; Sutter, E.; Batzill, M. Why is anatase a better photocatalyst than rutile?–Model studies on epitaxial TiO_2 films. *Sci. Rep.* **2014**, *4*, 4043.
(6) (a) Sung, Y.-M.; Kim, H.-J. Sputter deposition and surface treatment of TiO_2 films for dye-sensitized solar cells using reactive RF plasma. *Thin Solid Films* **2007**, *515*, 4996−4999. (b) Abbasi, S.; Hasanpour, M.; Ahmadpoor, F.; Sillanpää, M.; Dastan, D.; Achour, A. Application of the statistical analysis methodology for photo-degradation of methyl orange using a new nanocomposite containing modified TiO_2 semiconductor with SnO_2. *Int. J. Environ. Anal. Chem.* **2021**, *101*, 208−224. (c) Gundogdu, G.; Ulusoy Ghobadi, T. G.; Sadigh Akbari, S.; Ozbay, E.; Karadas, F. Photocatalytic water oxidation with a Prussian blue modified brown TiO_2. *J. Chem. Soc., Chem. Commun.* **2021**, *57*, 508−511.
(7) Meng, N.; Ren, X.; Santagiuliana, G.; Ventura, L.; Zhang, H.; Wu, J.; Yan, H.; Reece, M. J.; Bilotti, E. Ultrahigh β-phase content poly(vinylidene fluoride) with relaxor-like ferroelectricity for high energy density capacitors. *Nat. Commun.* **2019**, *10*, 4535.
(8) Chiodo, L.; García-Lastra, J. M.; Iacomino, A.; Ossicini, S.; Zhao, J.; Petek, H.; Rubio, A. Self-energy and excitonic effects in the electronic and optical properties of TiO_2 crystalline phases. *Phys. Rev. B: Condens. Matter Mater. Phys.* **2010**, *82*, 045207.
(9) Baldini, E.; Chiodo, L.; Dominguez, A.; Palummo, M.; Moser, S.; Yazdi-Rizi, M.; Auböck, G.; Mallett, B. P.; Berger, H.; Magrez, A.; Bernhard, C. Strongly bound excitons in anatase TiO_2 single crystals and nanoparticles. *Nat. Commun.* **2017**, *8*, 13.
(10) Lee, K.-M.; Suryanarayanan, V.; Ho, K.-C. A study on the electron transport properties of TiO_2 electrodes in dye-sensitized solar cells. *Sol. Energy Mater. Sol. Cells* **2007**, *91*, 1416−1420.
(11) Rao, M. C.; Ravindranadh, K.; Shekhawat, M. S. Structural and electrical properties of TiO_2 thin films. *AIP Conference Proceedings*; AIP Publishing LLC, 2016; Vol. *1728*, p 020077.
(12) Ito, S.; Ha, N.-L. C.; Rothenberger, G.; Liska, P.; Comte, P.; Zakeeruddin, S. M.; Péchy, P.; Nazeeruddin, M. K.; Grätze, l. M. High-efficiency (7.2%) flexible dye-sensitized solar cells with Ti-metal substrate for nanocrystalline-TiO_2 photoanode. *Chem. Commun.* **2006**, 4004−4006.
(13) Sasi, S.; Sugunan, S. K.; Radhakrishnan Nair, P.; Subramanian, K. R. V.; Mathew, S. Scope of surface-modified molecular and nanomaterials in gel/liquid forms for developing mechanically flexible DSSCs/QDSSCs. *Photochem. Photobiol. Sci.* **2019**, *18*, 15−29.
(14) Kuang, D.; Brillet, J.; Chen, P.; Takata, M.; Uchida, S.; Miura, H.; Sumioka, K.; Zakeeruddin, S. M.; Grätzel, M. Application of highly ordered TiO_2 nanotube arrays in flexible dye-sensitized solar cells. *ACS Nano* **2008**, *2*, 1113−1116.
(15) Shakeel Ahmad, M.; Pandey, A. K.; Abd Rahim, N. Advancements in the development of TiO_2 photoanodes and its fabrication methods for dye-sensitized solar cell (DSSC) applications. A review. *Renewable Sustainable Energy Rev.* **2017**, *77*, 89−108.
(16) Jena, A.; Mohanty, S. P.; Kumar, P.; Naduvath, J.; Gondane, V.; Lekha, P.; Das, J.; Narula, H. K.; Mallick, S.; Bhargava, P. Dye Sensitized Solar Cells: A Review. *Trans. Indian Ceram. Soc.* **2012**, *71*, 1−16.
(17) Mahmoud, M. S.; Akhtar, M. S.; Mohamed, I. M. A.; Hamdan, R.; Dakka, Y. A.; Barakat, N. A. M. Demonstrated photons to electron activity of S-doped TiO_2 nanofibers as photoanode in the DSSC. *Mater. Lett.* **2018**, *225*, 77−81.
(18) Lin, L.-Y.; Lee, C.-P.; Tsai, K.-W.; Yeh, M.-H.; Chen, C.-Y.; Vittal, R.; Wu, C.-G.; Ho, K.-C. Low-temperature flexible Ti/TiO_2 photoanode for dye-sensitized solar cells with binder-free TiO_2 paste. *Prog. Photovoltaics Res. Appl.* **2012**, *20*, 181−190.
(19) Zeng, Q.; Yu, Y.; Wu, L.; Qi, B.; Zhi, J. Low-temperature fabrication of flexible TiO_2 electrode for dye-sensitized solar cells. *Phys. Status Solidi A* **2010**, *207*, 2201−2206.
(20) Holliman, P. J.; Connell, A.; Davies, M.; Carnie, M.; Bryant, D.; Jones, E. W. Low temperature sintering of aqueous TiO_2 colloids for flexible, co-sensitized dye-sensitized solar cells. *Mater. Lett.* **2019**, *236*, 289−291.
(21) Lee, H.; Hwang, D.; Jo, S. M.; Kim, D.; Seo, Y.; Kim, D. Y. Low-temperature fabrication of TiO2 electrodes for flexible dye-sensitized solar cells using an electrospray process. *ACS Appl. Mater. Interfaces* **2012**, *4*, 3308−3315.
(22) (a) Weerasinghe, H. C.; Huang, F.; Cheng, Y.-B. Fabrication of flexible dye sensitized solar cells on plastic substrates. *Nano Energy* **2013**, *2*, 174−189. (b) Rezaei, B.; Mohammadi, I.; Ensafi, A. A.; Momeni, M. M. Enhanced efficiency of DSSC through AC-electrophoretic hybridization of TiO_2 nanoparticle and nanotube. *Electrochim. Acta* **2017**, *247*, 410−419.
(23) (a) Chiu, W.-H.; Lee, K.-M.; Hsieh, W.-F. High efficiency flexible dye-sensitized solar cells by multiple electrophoretic depositions. *J. Power Sources* **2011**, *196*, 3683−3687. (b) Al Abduljabbar, F. A.; Haider, S.; Ali, F. A. A.; Alghyamah, A. A.; Almasry, W. A.; Patel, R.; Mujtaba, I. M. Efficient Photocatalytic Degradation of Organic Pollutant in Wastewater by Electrospun Functionally Modified Polyacrylonitrile Nanofibers Membrane Anchoring TiO_2 Nanostructured. *Membranes* **2021**, *11*, 785.
(24) Zhang, J.-X.; Zheng, Y.-P.; Lan, L.; Mo, S.; Yu, P.-Y.; Shi, W.; Wang, R.-M. Direct Synthesis of Solvent-free Multiwall Carbon Nanotubes/Silica Nonionic Nanofluid Hybrid Material. *ACS Nano* **2009**, *3*, 2185−2190.
(25) (a) Li, H.; Babu, S. S.; Turner, S. T.; Neher, D.; Hollamby, M. J.; Seki, T.; Yagai, S.; Deguchi, Y.; Möhwald, H.; Nakanishi, T. Alkylated-C60 based soft materials: regulation of self-assembly and optoelectronic properties by chain branching. *J. Mater. Chem. C* **2013**, *1*, 1943−1951. (b) Shang, K.; Gao, J.; Yin, X.; Ding, Y.; Wen, Z. An Overview of Flexible Electrode Materials/Substrates for Flexible Electrochemical Energy Storage/Conversion Devices. *Eur. J. Inorg. Chem.* **2021**, *2021*, 606−619.
(26) (a) Santhosh Babu, S.; Nakanishi, T. Nonvolatile Functional Molecular Liquids. *Chem. Commun.* **2013**, *49*, 9373−9382. (b) Gupta, K.; Yasa, S. R.; Khan, A.; Sharma, O. P.; Khatri, O. P. Charge-driven interaction for adsorptive removal of organic dyes using ionic liquid-modified graphene oxide. *J. Colloid Interface Sci.* **2022**, *607*, 1973−1985. (c) Esmati, M.; Zeynizadeh, B. Synthesis of GO and rGO@Fe 3 O 4 @Ni as remarkable nanocatalyst systems for solvent-free and chemoselective coupling reactions of dimedone with aromatic aldehydes. *Appl. Organomet. Chem.* **2021**, *35*, 6321. (d) Azizi, S.; Shadjou, N. Iron oxide (Fe_3O_4) magnetic nanoparticles supported on wrinkled fibrous nanosilica (WFNS) functionalized by biimidazole ionic liquid as an effective and reusable heterogeneous magnetic nanocatalyst for the efficient synthesis of N-sulfonylamidines. *Heliyon* **2021**, *1*, No. e05915.
(27) Bourlinos, A.B.; Ray Chowdhury, S.; Herrera, R.; Jiang, D.D.; Zhang, Q.; Archer, L. A.; Giannelis, E.P. Functionalized nanostructures with liquid-like behavior: expanding the gallery of available nanostructures. *Adv. Funct. Mater.* **2010**, *15*, 1285−1290.
(28) Yu, P. Y.; Zheng, Y. P. The Synthesis of Solvent-Free TiO_2 Nanofluids through Surface Modification. *Soft Nanosci. Lett.* **2011**, *1*, 46−50.
(29) Zheng, Y.; Zhang, J.; Lan, L.; Yu, P.; Rodriguez, R.; Herrera, R.; Wang, D.; Giannelis, E. P. Preparation of solvent-free gold nanofluids with facile self-assembly technique. *ChemPhysChem* **2010**, *11*, 61−64.
(30) (a) Bidal, J.; Becuwe, M.; Hadad, C.; Fleutot, B.; Davoisne, C.; Deschamps, M.; Porcheron, B.; Nhien, A. N. V. Hybrid Electrolytes Based on Optimized Ionic Liquid Quantity Tethered on ZrO_2 Nanoparticles for Solid-State Lithium-Ion Conduction. *ACS Appl. Mater. Interfaces* **2021**, *13*, 15159−15167. (b) Moganty, S. S.; Jayaprakash, N.; Nugent, J. L.; Shen, J.; Archer, L. A. Ionic-Liquid-Tethered Nanoparticles: Hybrid Electrolytes. *Angew. Chem.* **2010**, *122*, 9344−9347. (c) Elmouwahidi, A.; Bailón-García, E.; Pérez-

https://doi.org/10.1021/acsomega.2c01425
ACS Omega 2022, 7, 25094−25109

Cadenas, A. F.; Maldonado-Hódar, F. J.; Castelo-Quibén, J.; Carrasco-Marín, F. Electrochemical performances of supercapacitors from carbon-ZrO_2 composites. *Electrochim. Acta* **2018**, *259*, 803−814. (d) Sasi, S.; Sugunan, S. K.; Radhakrishnan Nair, P.; Subramanian, K. R. V.; George, R.; Nageswara Rao, T.; Mathew, S. High power flexible supercapacitor electrodes based on a surface modified C_{60}−βNi-$(OH)_2$ nanocomposite. *Mater. Today Commun.* **2021**, *26*, 101825.

(31) Kim, J.-H.; Hossain, S. M.; Kang, H.-J.; Park, H.; Tijing, L.; Park, G. W.; Suzuki, N.; Fujishima, A.; Jun, Y.-S.; Shon, H. K.; Kim, G.-J. Hydrophilic/Hydrophobic Silane Grafting on TiO_2 Nanoparticles: Photocatalytic Paint for Atmospheric Cleaning. *Catalysts* **2021**, *11*, 193.

(32) Martinez-Oviedo, A.; Kshetri, Y. K.; Joshi, B.; Lee, S. W. Surface modification of blue TiO_2 with silane coupling agent for NOx abatement. *Prog. Nat. Sci.: Mater. Int.* **2021**, *31*, 230−238.

(33) Rokicka-Konieczna, P.; Wanag, A.; Sienkiewicz, A.; Kusiak-Nejman, E.; Morawski, A. W. Effect of APTES modified TiO_2 on antioxidant enzymes activity secreted by Escherichia coli and Staphylococcus epidermidis. *Biochem. Biophys. Res. Commun.* **2021**, *534*, 1064−1068.

(34) Dinari, M.; Haghighi, A. Surface modification of TiO_2 nanoparticle by three-dimensional silane coupling agent and preparation of polyamide/modified-TiO_2 nanocomposites for removal of Cr (VI) from aqueous solutions. *Prog. Org. Coat.* **2017**, *110*, 24−34.

(35) Kusiak-Nejman, E.; Sienkiewicz, A.; Wanag, A.; Rokicka-Konieczna, P.; Morawski, A. W. The Role of Adsorption in the Photocatalytic Decomposition of Dyes on APTES-Modified TiO_2 Nanomaterials. *Catalysts* **2021**, *11*, 172.

(36) Wanag, A.; Sienkiewicz, A.; Rokicka-Konieczna, P.; Kusiak-Nejman, E.; Morawski, A. W. Influence of modification of titanium dioxide by silane coupling agents on the photocatalytic activity and stability. *J. Environ. Chem. Eng.* **2020**, *8*, 103917.

(37) Takeshita, T. DFT and TD-DFT Study on Azobenzene-Based Dye Covalently Attached to Silane Coupling Agents: Toward Dye-Sensitized TiO_2 Catalyst and Dye-Sensitized Solar Cell Applications. *ChemistrySelect* **2021**, *6*, 6011−6018.

(38) Ukaji, E.; Furusawa, T.; Sato, M.; Suzuki, N. The effect of surface modification with silane coupling agent on suppressing the photo-catalytic activity of fine TiO_2 particles as inorganic UV filter. *Appl. Surf. Sci.* **2007**, *254*, 563−569.

(39) Sienkiewicz, A.; Rokicka-Konieczna, P.; Wanag, A.; Kusiak-Nejman, E.; Morawski, A. W. Artificial Solar Light-Driven APTES/TiO_2 Photocatalysts for Methylene Blue Removal from Water. *Molecules* **2022**, *27*, 947.

(40) Dadpanah, A.; Rabiee, A.; Mohammadi, F.; Ershad Langroudi, A.; Zeynali, M. E. Preparation and characterization of AM-co-APTAC/TiO_2 nanocomposite for environmental applications. *Polym. Bull.* **2022**, *79*, 1039−1055.

(41) Qian, J.; Ma, Q.; Xu, J. Surface modification of nanoparticles with octadecyl trichlorosilane and its effects on photocatalytic activity. *Micro Nano Lett.* **2013**, *8*, 115−118.

(42) Zhao, J.; Milanova, M.; Warmoeskerken, M. M. C. G.; Dutschk, V. Surface modification of TiO2 nanoparticles with silane coupling agents. *Colloids Surf., A* **2012**, *413*, 273−279.

(43) Bao, N.; Wu, G.; Niu, J.; Zhang, Q.; He, S.; Wang, J. Wide spectral response and enhanced photocatalytic activity of TiO_2 continuous fibers modified with aminosilane coupling agents. *J. Alloys Compd.* **2014**, *599*, 40−48.

(44) Yan, M.; Zeng, G.; Li, X.; Zhao, C.; Yang, G.; Gong, J.; Chen, G.; Tang, L.; Huang, D. Titanium dioxide nanotube arrays with silane coupling agent modification for heavy metal reduction and persistent organic pollutant degradation. *New J. Chem.* **2017**, *41*, 4377−4389.

(45) Hang, Y.; Yin, H.; Ji, Y.; Liu, Y.; Lu, Z.; Wang, A.; Shen, L.; Yin, H. Adsorption performances of naked and 3-aminopropyl triethoxysilane-modified mesoporous TiO_2 hollow nanospheres for Cu^{2+}, Cd^{2+}, Pb^{2+}, and Cr(VI) ions. *J. Nanosci. Nanotechnol.* **2017**, *17*, 5539−5549.

(46) Moreno-Hernandez, I. A.; MacFarland, C. A.; Read, C. G.; Papadantonakis, K. M.; Brunschwig, B. S.; Lewis, N. S. Crystalline nickel manganese antimonate as a stable water-oxidation catalyst in aqueous 1.0 MH $_2$ SO_4. *Energy. Environ. Sci.* **2017**, *10*, 2103−2108.

(47) Pai, N.; Lu, J.; Gengenbach, T. R.; Seeber, A.; Chesman, A. S. R.; Jiang, L.; Senevirathna, D. C.; Andrews, P. C.; Bach, U.; Cheng, Y. B.; Simonov, A. N. Silver bismuth sulfoiodide solar cells: tuning optoelectronic properties by sulfide modification for enhanced photovoltaic performance. *Adv. Energy Mater.* **2019**, *9*, 1803396.

(48) Luke, S.; Chatti, M.; Yadav, A.; Kerr, B. V.; Kangsabanik, J.; Williams, T.; Cherepanov, P. V.; Johannessen, B.; Tanksale, A.; MacFarlane, D. R.; Hocking, R. K.; Alam, A.; Yella, A.; Simonov, A. N. Mixed metal-antimony oxide nanocomposites: low pH water oxidation electrocatalysts with outstanding durability at ambient and elevated temperatures. *J. Mater. Chem. A* **2021**, *9*, 27468−27484.

(49) Ohsaki, Y.; Masaki, N.; Kitamura, T.; Wada, Y.; Okamoto, T.; Sekino, T.; Niihara, K.; Yanagida, S. Dye-sensitized TiO_2 nanotube solar cells: fabrication and electronic characterization. *Phys. Chem. Chem. Phys.* **2005**, *7*, 4157−4163.

(50) Zubavichus, Y. V.; Slovokhotov, Y. L.; Nazeeruddin, M. K.; Zakeeruddin, S. M.; Grätzel, M.; Shklover, V. Structural Characterization of Solar Cell Prototypes Based on Nanocrystalline TiO_2 Anatase Sensitized with Ru Complexes. X-ray Diffraction, XPS, and XAFS Spectroscopy Study. *Chem. Mater.* **2002**, *14*, 3556−3563.

(51) (a) Jing, L.; Li, S.; Song, S.; Xue, L.; Fu, H. Investigation on the electron transfer between anatase and rutile in nano-sized TiO_2 by means of surface photovoltage technique and its effects on the photocatalytic activity. *Sol. Energy Mater. Sol. Cells* **2008**, *92*, 1030−1036. (b) Sienkiewicz, A.; Wanag, A.; Kusiak-Nejman, E.; Ekiert, E.; Rokicka-Konieczna, P.; Morawski, A. W. Effect of calcination on the photocatalytic activity and stability of TiO_2 photocatalysts modified with APTES. *J. Environ. Chem. Eng.* **2021**, *9*, 104794.

(52) Ohtani, B.; Ogawa, Y.; Nishimoto, S.-i. Photocatalytic Activity of Amorphous−Anatase Mixture of Titanium(IV) Oxide Particles Suspended in Aqueous Solutions. *J. Phys. Chem. B* **1997**, *101*, 3746−3752.

(53) Kéri, O.; Kócs, L.; Hórvölgyi, Z.; Baji, Z.; László, K.; Takáts, V.; Erdélyi, Z.; Szilágyi, I. M. Photocatalytically active amorphous and crystalline TiO_2 prepared by atomic layer deposition. *Period. Polytech., Chem. Eng.* **2019**, *63*, 378−387.

(54) Ohtani, B.; Ogawa, Y.; Nishimoto, S.-i. Photocatalytic Activity of Amorphous−Anatase Mixture of Titanium(IV) Oxide Particles Suspended in Aqueous Solutions. *J. Phys. Chem. B* **1997**, *101*, 3746−3752.

(55) Jang, J. S.; Kim, H. G.; Ji, S. M.; Bae, S. W.; Jung, J. H.; Shon, B. H.; Lee, J. S. Formation of crystalline TiO_2− xNx and its photocatalytic activity. *J. Solid State Chem.* **2006**, *179*, 1067−1075.

(56) Lin, C.-P.; Chen, H.; Nakaruk, A.; Koshy, P.; Sorrell, C. C. Effect of Annealing Temperature on the Photocatalytic Activity of TiO_2 Thin Films. *Energy Procedia* **2013**, *34*, 627−636.

(57) Yu, J.; Dai, G.; Cheng, B. Effect of Crystallization Methods on Morphology and Photocatalytic Activity of Anodized TiO_2 Nanotube Array Films. *J. Phys. Chem. C* **2010**, *114*, 19378−19385.

(58) Liang, H.; Meng, Q.; Wang, X.; Zhang, H.; Wang, J. Nanoplasmonically Engineered Interfaces on Amorphous TiO_2 for Highly Efficient Photocatalysis in Hydrogen Evolution. *ACS Appl. Mater. Interfaces* **2018**, *10*, 14145−14152.

(59) Chu, L.; Qin, Z.; Yang, J.; Li, X. A. Anatase TiO_2 nanoparticles with exposed {001} facets for efficient dye-sensitized solar cells. *Sci. Rep.* **2015**, *5*, 12143.

(60) (a) Siah, W. R.; Lintang, H. O.; Shamsuddin, M.; Yuliati, L.; High photocatalytic activity of mixed anatase-rutile phases on commercial TiO_2 nanoparticles, *IOP Conference Series: Materials Science and Engineering*; IOP Publishing, 2016; Vol. *107*, p 012005. (b) Liu, Z.; Daali, A.; Xu, G.-L.; Zhuang, M.; Zuo, X.; Sun, C.-J.; Liu, Y.; Cai, Y.; Hossain, M. D.; Liu, H.; Amine, K.; Luo, Z. Highly reversible sodiation/desodiation from a carbon-sandwiched SnS_2 nanosheet anode for sodium-ion batteries. *Nano Lett.* **2020**, *20*, 3844−3851.

https://doi.org/10.1021/acsomega.2c01425
ACS Omega 2022, 7, 25094−25109

(61) Almeida, A. R.; Calatayud, M.; Tielens, F.; Moulijn, J. A.; Mul, G. Combined ATR-FTIR and DFT study of cyclohexanone adsorption on hydrated TiO_2 anatase surfaces. *J. Phys. Chem. C* **2011**, *115*, 14164−14172.
(62) Sewvandi, G. A.; Tao, Z.; Kusunose, T.; Tanaka, Y.; Nakanishi, S.; Feng, Q. Modification of TiO_2 electrode with organic silane interposed layer for high-performance of dye-sensitized solar cells. *ACS Appl. Mater. Interfaces* **2014**, *6*, 5818−5826.
(63) Ni, W.; Wu, S.; Ren, Q. Preparation and characterization of silanized TiO_2 nanoparticles and their application in toner. *Ind. Eng. Chem. Res.* **2012**, *51*, 13157−13163.
(64) De Angelis, F.; Fantacci, S.; Mosconi, E.; Nazeeruddin, M. K.; Grätzel, M. Absorption spectra and excited-state energy levels of the N719 dye on TiO_2 in dye-sensitized solar cell models. *J. Phys. Chem. C* **2011**, *115*, 8825−8831.
(65) Gotić, M.; Ivanda, M.; Popović, S.; Musić, S.; Sekulić, A.; Turković, A.; Furić, K. Raman investigation of nanosized TiO_2. *J. Raman Spectrosc.* **1997**, *28*, 555−558.
(66) Doğan, İ.; van de Sanden, M. C. Direct characterization of nanocrystal size distribution using Raman spectroscopy. *J. Appl. Phys.* **2013**, *114*, 134310.
(67) Murugan, A. V.; Samuel, V.; Ravi, V. Synthesis of nanocrystalline anatase TiO_2 by microwave hydrothermal method. *Mater. Lett.* **2006**, *60*, 479−480.
(68) Xu, N.; Shi, Z.; Fan, Y.; Dong, J.; Shi, J.; Hu, M. Z.-C. Effects of particle size of TiO_2 on photocatalytic degradation of methylene blue in aqueous suspensions. *Ind. Eng. Chem. Res.* **1999**, *38*, 373−379.
(69) Zuo, R.; Du, G.; Zhang, W.; Liu, L.; Liu, Y.; Mei, L.; Li, Z. Photocatalytic degradation of methylene blue using TiO_2 impregnated diatomite. *Adv. Mater. Sci. Eng.* **2014**, *2014*, 170148.
(70) Huang, L.; Peng, F.; Ohuchi, F. S. "In situ" XPS study of band structures at Cu_2O/TiO_2 heterojunctions interface. *Surf. Sci.* **2009**, *603*, 2825−2834.
(71) Ansari, S. A.; Ansari, M. O.; Cho, M. H. Facile and scale-up synthesis of red phosphorus-graphitic carbon nitride heterostructures for energy and environment applications. *Sci. Rep.* **2016**, *6*, 27713.
(72) Sun, P.; Liu, G.; Lv, D.; Dong, X.; Wu, J.; Wang, D. Effective activation of halloysite nanotubes by piranha solution for amine modification via silane coupling chemistry. *RSC Adv.* **2015**, *5*, 52916−52925.
(73) Wagner, C. D.; Naumkin, A. V.; Kraut-Vass, A.; Allison, J. W.; Powell, C. J.; Rumble, J. R., Jr. *NIST Standard Reference Database 20, Version 3.4 (Web version)*; National Institute of Standards and Technology: Gaithersburg, MD, 2003; p 20899.
(74) Meškinis, Š.; Vasiliauskas, A.; Andrulevičius, M.; Peckus, D.; Tamulevičius, S.; Viskontas, K. Diamond like carbon films containing Si: structure and nonlinear optical properties. *Materials* **2020**, *13*, 1003.
(75) Rimoldi, L.; Meroni, D.; Pargoletti, E.; Biraghi, I.; Cappelletti, G.; Ardizzone, S. Role of the growth step on the structural, optical and surface features of TiO_2/SnO_2 composites. *R. Soc. Open Sci.* **2019**, *6*, 181662.
(76) Jubu, P. R.; Yam, F. K.; Igba, V. M.; Beh, K. P. Tauc-plot scale and extrapolation effect on bandgap estimation from UV−vis−NIR data−a case study of β-Ga_2O_3. *J. Solid State Chem.* **2020**, *290*, 121576.
(77) Zheng, D.; Xiong, J.; Guo, P.; Li, Y.; Gu, H. Fabrication of improved dye-sensitized solar cells with anatase/rutile TiO_2 nanofibers. *J. Nanosci. Nanotechnol.* **2016**, *16*, 613−618.
(78) Liqiang, J.; Yichun, Q.; Baiqi, W.; Shudan, L.; Baojiang, J.; Libin, Y.; Wei, F.; Honggang, F.; Jiazhong, S. Review of photoluminescence performance of nano-sized semiconductor materials and its relationships with photocatalytic activity. *Sol. Energy Mater. Sol. Cells* **2006**, *90*, 1773−1787.
(79) Tian, F.; Zhang, Y.; Zhang, J.; Pan, C. Raman spectroscopy: a new approach to measure the percentage of anatase TiO_2 exposed (001) facets. *J. Phys. Chem. C* **2012**, *116*, 7515−7519.
(80) Hu, Y.; Song, X.; Jiang, S.; Wei, C. Enhanced photocatalytic activity of Pt-doped TiO_2 for NOx oxidation both under UV and visible light irradiation: A synergistic effect of lattice Pt^{4+} and surface PtO. *Chem. Eng. J.* **2015**, *274*, 102−112.
(81) Choudhury, B.; Choudhury, A. Oxygen defect dependent variation of band gap, Urbach energy and luminescence property of anatase, anatase-rutile mixed phase and of rutile phases of TiO_2 nanoparticles. *Phys. E* **2014**, *56*, 364−371.
(82) (a) Wu, M.-C.; Chan, S.-H.; Jao, M.-H.; Su, W.-F. Enhanced short-circuit current density of perovskite solar cells using Zn-doped TiO_2 as electron transport layer. *Sol. Energy Mater. Sol. Cells* **2016**, *157*, 447−453. (b) Wang, X.; Feng, Z.; Shi, J.; Jia, G.; Shen, S.; Zhou, J.; Li, C. Trap states and carrier dynamics of TiO_2 studied by photoluminescence spectroscopy under weak excitation condition. *Phys. Chem. Chem. Phys.* **2010**, *12*, 7083−7090. (c) Deák, P.; Aradi, B.; Frauenheim, T. Band lineup and charge carrier separation in mixed rutile-anatase systems. *J. Phys. Chem. C* **2011**, *115*, 3443−3446.
(83) Huang, Y.; Shu, S.; Lu, Z.; Fan, Y. Characterization of the adhesion of thin palladium membranes supported on tubular porous ceramics. *Thin Solid Films* **2007**, *515*, 5233−5240.
(84) Heger, D.; Jirkovský, J.; Klán, P. Aggregation of methylene blue in frozen aqueous solutions studied by absorption spectroscopy. *J. Phys. Chem. A* **2005**, *109*, 6702−6709.
(85) Kulkarni, S. A.; Ogale, S. B.; Vijayamohanan, K. P. Tuning the hydrophobic properties of silica particles by surface silanization using mixed self-assembled monolayers. *J. Colloid Interface Sci.* **2008**, *318*, 372−379.
(86) Cavalcante, R. P.; Dantas, R. F.; Bayarri, B.; González, O.; Giménez, J.; Esplugas, S.; Machulek, A. Synthesis and characterization of B-doped TiO_2 and their performance for the degradation of metoprolol. *Catal. Today* **2015**, *252*, 27−34.
(87) (a) Zhang, J.; Nosaka, Y. Mechanism of the OH radical generation in photocatalysis with TiO_2 of different crystalline types. *J. Phys. Chem. C* **2014**, *118*, 10824−10832. (b) Nosaka, Y.; Nosaka, A. Understanding Hydroxyl Radical (OH) Generation Processes in Photocatalysis. *ACS Energy Lett.* **2016**, *1*, 356−359.
(88) Wang, Y.; Wu, Q.; Li, Y.; Liu, L.; Geng, Z.; Li, Y.; Chen, J.; Bai, W.; Jiang, G.; Zhao, Z. Controlled fabrication of TiO_2/C_3N_4 core-shell nanowire arrays: a visible-light-responsive and environmental-friendly electrode for photoelectrocatalytic degradation of bisphenol A. *J. Mater. Sci.* **2018**, *53*, 11015−11026.
(89) Suay, J. J.; Giménez, E.; Rodríguez, T.; Habbib, K.; Saura, J. J. Characterization of anodized and sealed aluminium by EIS. *Corros. Sci.* **2003**, *45*, 611−624.

https://doi.org/10.1021/acsomega.2c01425
ACS Omega 2022, 7, 25094−25109